# We are IntechOpen, the world's leading publisher of Open Access books
# Built by scientists, for scientists

**4,800**
Open access books available

**122,000**
International authors and editors

**135M**
Downloads

Our authors are among the

**154**
Countries delivered to

**TOP 1%**
most cited scientists

**12.2%**
Contributors from top 500 universities

CLARIVATE ANALYTICS
BOOK CITATION INDEX
INDEXED

WEB OF SCIENCE™

Selection of our books indexed in the Book Citation Index in Web of Science™ Core Collection (BKCI)

## Interested in publishing with us?
## Contact book.department@intechopen.com

Numbers displayed above are based on latest data collected.
For more information visit www.intechopen.com

7

# Mechanical Properties of Ceramics by Indentation: Principle and Applications

Didier Chicot[1] and Arnaud Tricoteaux[2]
*1) Laboratory of Mechanics, University of Science and Technology of Lille,*
*2) Laboratory of Materials and Process, University of Valenciennes and Hainaut Cambrésis, France*

## 1. Introduction

Mechanical properties such as hardness, bulk modulus, tensile properties and toughness of massive ceramics and adhesion or cohesion of ceramic coatings can be determined by indentation tests. From a general point of view, the indentation test simply consists of performing a print at the surface of a material by the penetration of a hard indenter at a given indentation load. For this purpose, the indenter can have different geometrical shapes such as spherical, conical or pyramidal, the objective being to produce a different elastoplastic deformation of the material below the indenter. The indentation load can be chosen in the nano-, micro- or macro-indentation ranges thus allowing the study of local or global mechanical properties. The mechanical properties are determined by analysing the geometrical dimensions of the residual indent (usual indentation) or from the analysis of a load-depth curve (instrumented indentation tests). Generally, pyramidal indenters are used to determine hardness, bulk modulus and cracking resistance of the material, whereas spherical indenters are mainly used to determine the tensile properties and bulk modulus. The objective of this chapter is to give theoretical and experimental tools for determining the mechanical properties by indentation of massive ceramics and ceramic coatings. The chapter is divided in five parts: 1) Hardness definition, indentation size effect, dynamic hardness and hardness of thin films, 2) Bulk modulus of massive materials using the Marshall's method and the Oliver and Pharr's method, spherical and Vickers indentations and bulk modulus modelling for thin films, 3) Vickers indentation fracture toughness, 4) Tensile mechanical properties and 5) Adhesive properties by scratch tests for thin films and interface indentation tests for thick coatings.

## 2. Hardness

### 2.1 Definition

The hardness of a material represents its resistance to plastic deformation usually by indentation. The general relation to calculate a hardness number is given by:

$$H = \frac{P}{A} \tag{1}$$

where H is the hardness number, P the applied load and A, a representative area of the residual indent.

For usual indentation, the hardness number can be calculated considering the true or the projected contact area. Indeed, the true contact area is used for Vickers (pyramidal square based) indentation, HV, whereas the projected contact area is used for both Meyer hardness, Hm, also using a Vickers indenter and for Knoop (pyramidal lozenge based) indentation, $HK_P$. Depending on the geometrical dimensions of the indenter, the hardness calculation is related to the Vickers indent diagonal, d, and to the large diagonal of the Knoop indent, L, according to the hardness definitions (Table 1).

| | True contact area | Projected contact area |
|---|---|---|
| Vickers indenter | $HV = 1.8544\frac{P}{d^2}$ | $Hm = 2\frac{P}{d^2}$ |
| Knoop indenter | $HK_T = 12.873\frac{P}{L^2}$ | $HK_P = 14.229\frac{P}{L^2}$ |

Table 1. Hardness calculation considering true or projected contact area for Vickers and Knoop indentions.

Note that in Table 1, the Knoop hardness, $HK_T$, is not a conventional hardness number. On the other hand, direct comparison between, as actually performed, Vickers hardness and Knoop hardness is not possible, whereas it is correct when considering the Meyer hardness. Nevertheless, for a valid comparison between Vickers and Knoop hardness numbers, Chicot et al. (2007a) suggested the consideration of the true contact area in the Knoop hardness calculation, i.e. $HK_T$. Figure 1a shows a typical comparison of hardness data deduced from indentation of different ceramics (Mukhopadhyay et al., 1990; Ullner et al., 2001 & 2002; Gong et al., 2002).

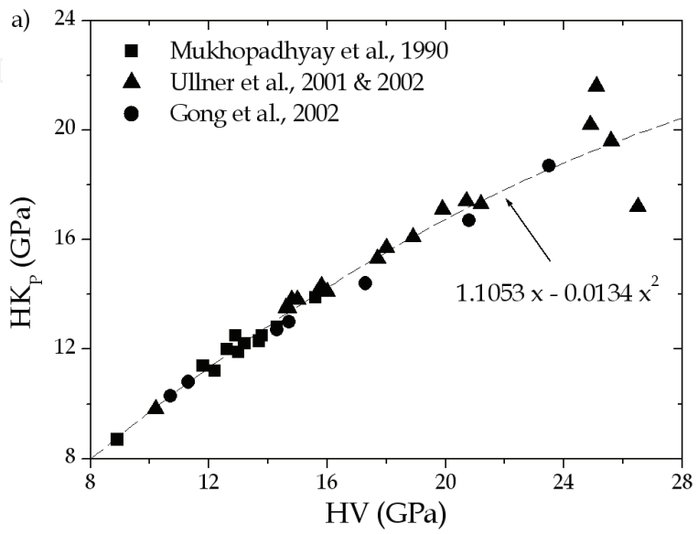

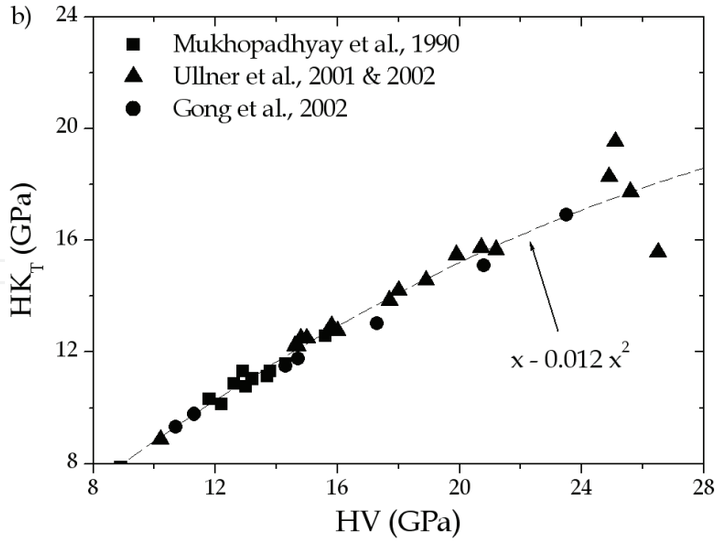


Fig. 1. Knoop hardness number as a function of Vickers hardness number for a variety of ceramics, where HK is calculated considering the projected contact area, $HK_P$, (a) or the true contact area, $HK_T$, (b).

Figure 1a shows that the conventional Knoop hardness number, $HK_P$, can be represented as a function of the Vickers hardness number, HV, by a second order polynomial, as follows:

$$HK_P = 1.1053 \cdot HV - 0.0134 \cdot HV^2 \tag{2}$$

The solution of this equation is obtained when the limit hardness, i.e. $H_{lim}$, is equal to 7.9 GPa, which respects the two following conditions:

$$\begin{aligned} &\text{If } HV < H_{lim} \text{ then } HK_P > HV \\ &\text{If } HV > H_{lim} \text{ then } HK_P < HV \end{aligned} \tag{3}$$

In any case, existence of such limit hardness has no physical justification. On the other hand, in fig. 1b the Knoop hardness number, $HK_T$, is expressed as a function of the Vickers hardness number, HV, by the polynomial:

$$HK_T = HV - 0.012 \cdot HV^2 \tag{4}$$

It is noticeable that the fitting coefficient in front of HV in eq. 4 is equal to 1. Nevertheless, this result was expected since the theoretical ratio to convert $HK_P$ to $HK_T$ is given by (14.229/12.873) = 1.1053 (see Table 1), which is the coefficient appearing in eq. 2. As a main conclusion, the two hardness numbers are the same only when the hardness value tends to zero. Consequently, no surprising change of the hardness will occur over the entire range of the hardness data.

For instrumented indentation tests (IIT), which allow the plot of a load-depth curve, the calculation of a hardness number can use the maximum distance (*maximum indentation depth,* $h_m$, *reached by the indenter during the indentation test*), the residual depth (*indentation depth,* $h_r$,

*obtained after the complete withdrawal of the indenter*) or the contact depth *(indentation depth,* $h_c$*, taking into account the deformation of the indent under load and calculated using the method of Oliver and Pharr (1992)*). Consequently, the hardness calculation can have different forms (Table 2) according to the indentation depth which is considered. As a result, comparison with hardness data obtained by several laboratories is somewhat difficult, even impossible if the hardness calculation is not well specified.

| Indentation depth | Maximum | Residual | Contact |
|---|---|---|---|
| True contact area | $HM = \frac{P}{26.43 h_m^2}$ | $H = \frac{P}{26.43 h_r^2}$ | $H = \frac{P}{26.43 h_c^2}$ |
| Projected contact area | $H = \frac{P}{24.5 h_m^2}$ | $H = \frac{P}{24.5 h_r^2}$ | $HIT = \frac{P}{24.5 h_c^2}$ |

Table 2. Hardness numbers considering true or projected contact areas and different indentation depth definitions.

To visualize the indentation depths, figure 2a represents schematically the cross-section of an indent and figure 2b shows the corresponding calculation of the indentation depths based on the analysis of a load-depth curve (Oliver and Pharr, 1992).

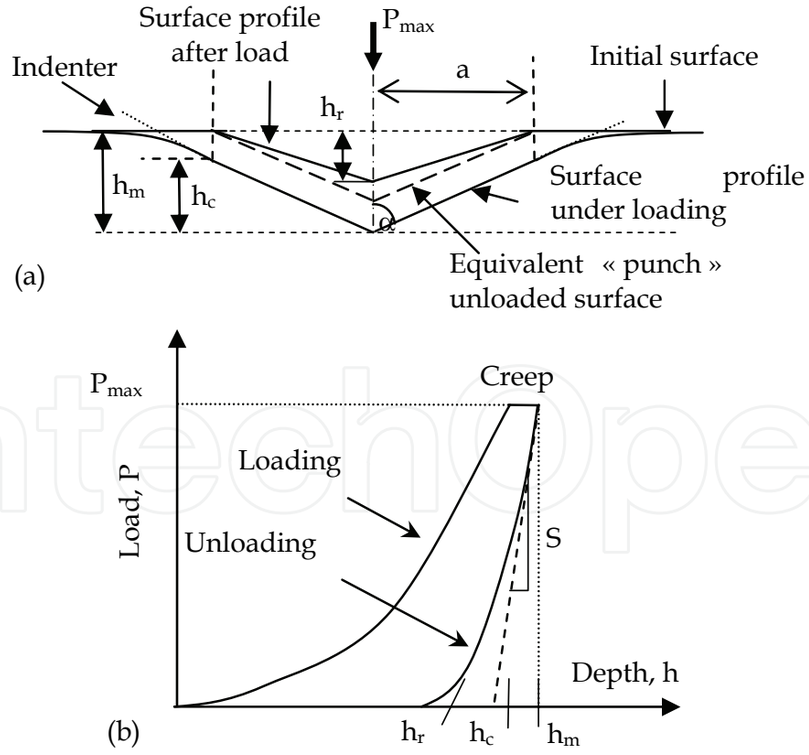


Fig. 2. (a) Schematic cross-section of a conical indent and (b) Load-depth curve and indentation depths used to calculate the hardness numbers.

Note that the Martens hardness, HM, and the contact hardness, HIT, are mainly used in micro and nano-indentation, respectively. The others hardness numbers are only given as a possibility of hardness calculation. In addition, HM is equivalent to HV if considering the diagonal to depth ratio of a Vickers indenter. As a conclusion, the different possibilities for calculating a hardness number must oblige the authors to specify correctly the hardness calculation (indenter type, contact area and the indentation depth), in order to have a sound discussion on the hardness behaviour of the material.

### 2.2 Indentation Size Effect

Whatever the shape of the indenter, the hardness number could be independent of load, it could increase or decrease with load, and it could show a complex variation with load changes depending on the material. This hardness-load dependence is known as the Indentation Size Effect (ISE). This phenomenon has been associated with various causes such as work hardening, roughness, piling-up, sinking-in, shape of the indenter, surface energy, varying composition and crystal anisotropy, which have been all discussed extensively by Cheng and Cheng (2004). Many relationships collected in a non-exhaustive list in table 3 (Chicot et al., 2007b), dating from 1885 to the present, have been suggested to describe the hardness-load dependence by expressing the applied load, P, as a function of the indent diagonal, d, or the hardness, H, as a function of the indentation depth, h.

| Equations: Polynomial laws | Referring | Equations: Strain Gradient Plasticity Theory | Referring |
|---|---|---|---|
| $P = A_0 \cdot d^2$ ..... | Kick, 1885 | $\frac{H}{H_0} = \sqrt{1 + \frac{h^*}{h}}$ ..... | Nix & Gao, 1998 |
| $P = A_1 \cdot d^n$ ..... | Meyer, 1908 | | |
| $P - W = A_2 \cdot d^2$ ..... | Hays & Kendall, 1973 | $\frac{H}{H_0} = 1 + \sqrt{\frac{h^*}{h}}$ ..... | Chong & Lam, 1999 |
| $P = c_0 + c_1 d + c_2 d^2 + \cdots + c_n d^n$ | Bückle, 1973 | | |
| $P = A_3 \cdot (d + d_0)^2$ ..... | Bull et al., 1989 | $\begin{cases} H = H_0 \sqrt{1 + \frac{h^*}{h}} + H_1 \\ H = H_0 \left( 1 + \sqrt{\frac{h^*}{h}} \right) + H_1 \end{cases}$, | Qiu et al., 2001 |
| $P = A_4 d + B_4 d^2$ ..... | Li & Bradt, 1993 | | |
| $Pd = w_1 d^2 + w_2 d^3$ ..... | Gong et al., 1999 | | |
| $P = c_0 + c_1 d + c_2 d^2$ ..... | Sangwal et al., 2002 | $H_1 = g \cdot \frac{f}{h}$ | |
| | | $\left( \frac{H}{H_0} \right)^{\beta} = 1 + \left( \frac{h^*}{h} \right)^{\beta/2}$ ..... | Abu Al-Rub, 2004 |

Table 3. Parametric laws for modelling the Indentation Size Effect.

By analysing experimental hardness results, the majority of these relations are able to adequately represent the hardness-load dependence from a mathematical point of view. However, when studying ISE in nano and micro-indentation, it is observed that the fitting parameters and the theoretical ones change without any clear justification. Then, to explain this difference, Chicot (2009) suggested the use of a hardness-length scale factor based on the strain gradient plasticity theory formerly proposed by Nix and Gao (1998). These authors showed that the ISE behaviour of crystalline materials can be accurately modelled

by introducing the concept of geometrically necessary dislocations (GND) based on Taylor's dislocation theory. They based their reasoning on the experimental law needed to advance a mechanism-based theory of strain gradient plasticity. The relation between the hardness and the indentation depth is:

$$\left(\frac{H}{Ho}\right)^2 = 1 + \left(\frac{h^*}{h}\right) \tag{5}$$

where Ho is the macro-hardness and h* the characteristic scale-length representing the hardness-load dependence.
Nix and Gao (1998) assumed for simplicity that the indentation deformation process is accommodated by geometrically necessary dislocations which are required to account for the permanent shape change at the surface. In these conditions, the macro-hardness and the characteristic scale-length of eq. 5 are expressed as follows:

$$Ho = \frac{3\sqrt{3}}{2}\mu b\sqrt{\rho_s} \quad \text{and} \quad h^* = \frac{81}{8}\frac{1}{f^3} b \tan^2\theta \left(\frac{\mu}{Ho}\right)^2 \tag{6}$$

where μ is the shear modulus, b the Burger's vector, $\rho_s$ the density of statistically stored dislocations and θ is equal to 19.3°. f is a corrective factor introduced by Durst et al. (2005) to take into account the GND effect on the size of the plastic zone. The factor f is equal to 1 in micro-indentation whereas it is equal to 1.9 for Durst et al. (2005) and to 1.44 for Nix and Gao (1998) in nano-indentation.
However, no direct comparison between the two couples $(Ho, h^*)_{micro}$ in micro-indentation and $(Ho, h^*)_{nano}$ in nano-indentation can be concluded due to the presence of the dislocation density which is not easily accessible prior to the indentation test and due to the relationship between h* and Ho, as shown in eq. 6. For these reasons, Chicot (2009) suggested the study of the indentation behaviour at the two scales of measurement by expressing the square of the hardness versus the reciprocal of the indentation depth. The slope, expressed as a function of the macro-hardness and the characteristic scale-length, is then proportional to an indentation toughness expressed in $MPa.m^{1/2}$. This parameter is called the hardness length-scale factor, $H_{LSF}$, which is equivalent to:

$$H_{LSF} = H_o\sqrt{h^*} \quad \text{when} \quad H^2 = H_o^2 + \frac{\left(H_o\sqrt{h^*}\right)^2}{h} \tag{7}$$

Then, by using eq. 6 and taking f equal to 1 in micro-indentation and 1.44 for nano-indentation according to Nix and Gao (1998), the hardness length-scale factor is simply written as a proportionality function of the shear modulus and the Burger's vector as follows:

$$H_{LSFmicro} = 1.14 \cdot \mu\sqrt{b} \quad \text{and} \quad H_{LSFnano} = 0.66 \cdot \mu\sqrt{b} \tag{8}$$

It is important to add that eq. 8 is only applicable for crystals. For other types of materials, eq. 7 is always appropriate but the hardness length-scale factor can only be used for

representing the ability of the material to deform by indentation but not for determining the above mentioned intrinsic parameters. However, the experimental hardness length-scale factor can be plotted as a function of the theoretical product $\mu.b^{1/2}$ for some indentation data obtained on various crystals using nano and micro-indentation experiments (Chicot, 2009). Figure 3 shows two straight lines with proportionality factors of 1.17 and 0.65 for micro-indentation and nano-indentation, respectively. These results agree very well with the theory (eq. 8).

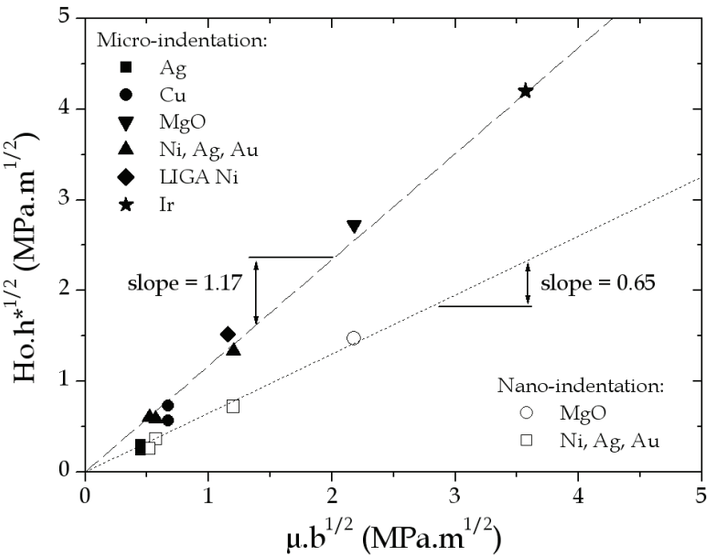


Fig. 3. Hardness length-scale factor, $Ho.h^{*1/2}$, as a function of the product, $\mu.b^{1/2}$, for various crystals.

As an example, we analysed the indentation size effect of a free porosity beta tricalcium phosphate bioceramic (called dense β-TCP ceramic in the following). The models of Meyer (1908), Li & Bradt (1993), Chong & Lam (1999) and Nix & Gao (1998) have been selected from the list (Table 3) and applied. Figure 4 shows that the models can adequately represent the ISE.

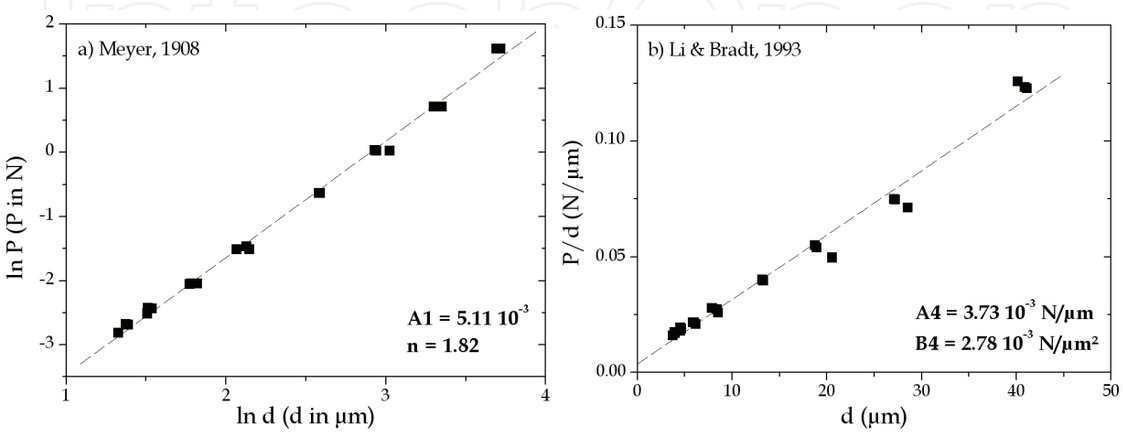

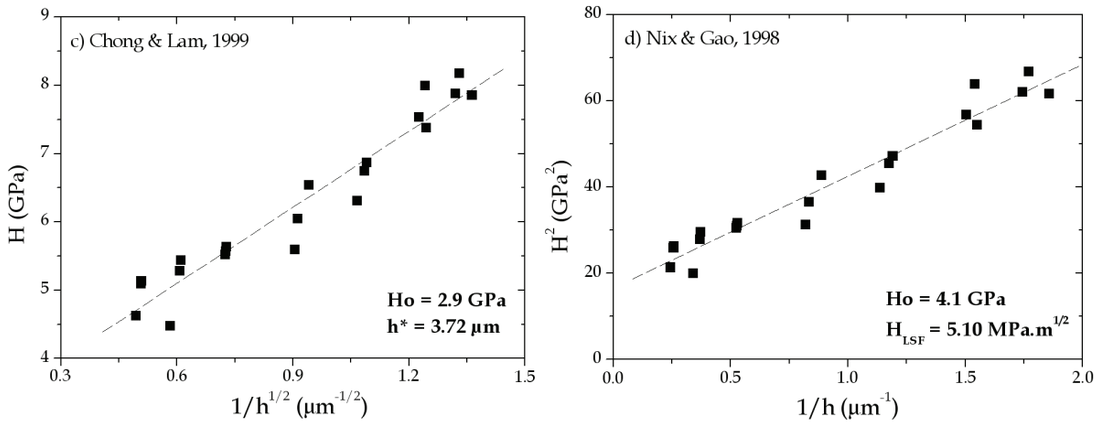


Fig. 4. Models of Meyer (1908) (a), Li & Bradt (1993) (b), Chong & Lam (1999) (c) and Nix & Gao (1998) (d) to represent the indentation size effect of the dense β-TCP ceramic.

Nevertheless, we prefer to use the model of Nix and Gao (1998) by introducing the hardness length-scale factor, which gives additional information about the ability of the material to deform plastically (Chicot, 2009).

### 2.3 Dynamic hardness

Usually the loading part of a load-depth curve (Fig. 2b) performed with a sharp indenter is described by a simple parabolic relationship between the applied load and the indentation depth of the form:

$$P = C_1 \cdot h^2 \tag{9}$$

where $C_1$ is a constant which depends on the geometry of the indenter tip and the material properties.

The validity of this relation has been demonstrated by means of numerical analysis of elastic-perfectly plastic and elastic-plastic materials (Giannkopoulos et al., 1994; Larsson et al., 1996; Giannakopoulos & Larsson, 1997; Briscoe et al., 1994; Bilodeau, 1992). Depending on the mechanical behaviour of the material, constant $C_1$ takes different forms expressed as a function of the elastic properties, yielding stress and stress measured at 29 % of strain of the material. However, numerous results (Giannkopoulos et al., 1994; Larsson et al., 1996; Giannakopoulos & Larsson, 1997) have shown that the experimental load-indentation depth relationship deviates from eq. 9 and that a better fit of the loading curve can be obtained by a more general power law taking a similar form of the Meyer's law (Meyer, 1908):

$$P = C_2 \cdot h^n \tag{10}$$

where $C_2$ is a material constant and n an exponent generally found to be less than 2.

Thus, the discrepancy between the experimental data and the theoretical description compromises the validity of the material properties derived from the loading curves analysis. Zeng and Chiu (2001) explained that the difference arises from the influence of the tip indenter defects. As a consequence, due to the rounding up of a sharp tip indenter, the initial part of the loading curve corresponding to the lowest indentation depth could be

modelled assuming that the indenter behaves as a spherical one. According to different authors, this approach is valid for the first 20-50 data points of the loading curve. For this region, the following relation could be applied:

$$P = C_3 \cdot h^{3/2} \tag{11}$$

where constant $C_3$ can be determined from fitting of the experimental data.
Beyond this point and until the maximum applied load, the authors consider a sharp indentation, but they introduce a constant $P_0$ to obtain a better fit of the second part of the loading curve, such that:

$$P = P_0 + C_4 \cdot h^2 \tag{12}$$

where $P_0$ and $C_4$ are also determined from the experimental data corresponding to this part of the curve.
The constant $P_0$ represents the initial deviation, which may arise from the initial contact load definition at the surface and/or due to the indenter tip imperfection. In micro-indentation, the influence of the indenter tip geometry is less pronounced than in nano-indentation since the influence of the rounded tip is sensitive only within a range of approximately 30 to 50 nm, depending on the size of such a defect (Chicot, 2009). For this reason, eq. 12 can be applied in micro-indentation over the entire loading curve by neglecting the effect of the rounded tip indenter. To consider the possible deviation of the zero contact, the constant load $P_0$ is introduced into the equation related to the Martens hardness definition (Table 2) in order to calculate a "dynamic" Martens hardness by considering the indentation depth reached by the indenter during the indentation:

$$HM = \frac{(P - P_0)}{26.43 \cdot h^2} \tag{13}$$

Then, by introducing eq. (12) into eq. (13), the dynamic Martens hardness becomes:

$$HM = \frac{C_4}{26.43} \tag{14}$$

which allows the relationship of constant $C_4$ with hardness. As a result, the hardness number is constant.
In order to take into account the indentation size effect, Chicot et al. (2010a) introduced eq. 7, expressing the Martens hardness as a function of the hardness length-scale factor, into the eq. 14 to express $C_4$ and, thereafter, into the eq. 12 to finally obtain the indentation loading curve function as follows:

$$P = P_0 + 26.43 \cdot \left( HM_0^2 + \frac{H_{LSF}^2}{h} \right)^{1/2} \cdot h^2 \tag{15}$$

As a conclusion, the proposed model representing the applied load (P) as a function of the indentation depth (h) involves three parameters: (*i*) the dynamic Martens macro-hardness ($HM_0$), (*ii*) the hardness length-scale factor ($H_{LSF}$) and (*iii*) a corrective load ($P_0$), considering the rounded tip effect of the indenter and the zero shifts.
The model is applied on the dense β-TCP ceramic. Figure 5 shows that eq. 15 adequately represents the loading curve and allows the determination of ISE parameters very close to those presented in figure 4d. Note that this methodology requires only one loading curve whereas classical approaches to study ISE require numerous indentation experiments to be accurate.

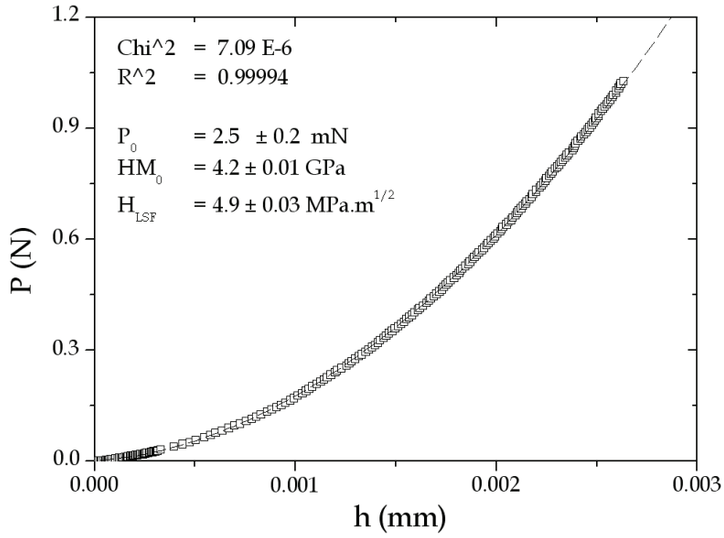


Fig. 5. Modelling of the loading curve (eq. 15) and values of the fitting parameters.

### 2.4 Hardness of thin films

For thin coated materials, direct measurement of the film hardness using conventional micro-hardness testers is not possible for a large range of indentation loads because the substrate undergoes a part of the plastic deformation during the indentation process. This phenomenon interferes when the indentation depth exceeds one tenth of the film thickness (Sun et al., 1995). In this case, the measured hardness number $H_C$ is the result of the two contributions of the film and of the substrate. Then, to determine the true film hardness it is necessary to separate these two contributions. Numerous models suppose a linear additive law to express the measured hardness, $H_C$, as a function of the film hardness, $H_F$, and of the substrate hardness, $H_S$, as follows:

$$H_C = H_S + a \cdot (H_F - H_S) \tag{16}$$

where the film coefficient, a, is associated with the film contribution.
The difference between the models comes from the expression describing the variation of the coefficient, a, as a function of the indent diagonal, the film thickness and elastic properties of both the film and the substrate. One of the earliest works was that of Bückle (1973), who defined the coefficient as a function of weighting factors associated with the volume of each layer of an influence zone affected by the indentation. Later, a more

successful model was due to Jönsson and Hogmark (1984), which considered the load supporting areas under the indent associated with the substrate and the film. From geometrical considerations, these authors expressed the film coefficient by the following relation:

$$a = C\left(\frac{t}{d}\right) - C^2\left(\frac{t}{d}\right)^2 \tag{17}$$

where t is the film thickness and d the indent diagonal. C is a constant equals to 1 for low $H_F/H_S$ (ductile films) and 0.5 for high $H_F/H_S$ (brittle films).
Considering that this model does not represent the real deformation behaviour during indentation, other authors have searched to link the film coefficient to the volumes of the plastic zones developed under the indent. This was proposed originally by Sargent (1979), followed by Burnett and Rickerby (1987a, 1987b) and Bull and Rickerby (1990) who used an interface parameter $\chi$ calculated from the following relations:

$$a = \frac{V_F}{V} \text{ with } V = V_F + \chi \cdot V_S \text{ and } \chi \propto \left(\frac{E_F \cdot H_S}{E_S \cdot H_F}\right)^q \text{ for } H_F > H_S \tag{18}$$

where $E_F$ and $E_S$ are the elastic modulus of the film and substrate, respectively. Nevertheless, the exponent q and, as a consequence, $\chi$, could be considered as adjustment parameters.
In order to avoid the introduction of such fitting parameters, Chicot and Lesage (1995) proposed a model based on the superposition of two hypothetic systems representing the volumes of the plastic deformation in the film and in the substrate under the indent. The mathematical development led to the following expression:

$$a = \frac{3}{2}\left(\frac{t}{d}\right)\left(\pi \cdot tg\xi\right)^{1/3}\left[\left(\frac{H_F}{E_F}\right)^{1/2} + \left(\frac{H_S}{E_S}\right)^{1/2}\right] - 2\left(\frac{t}{d}\right)^3\left(\pi \cdot tg\xi\right)\left[\left(\frac{H_F}{E_F}\right)^{3/2} + \left(\frac{H_S}{E_S}\right)^{3/2}\right] \tag{19}$$

where $\xi$ is the indenter semi-angle (74°). In addition, when the diagonal length is higher than that of the thickness, the second term becomes negligible.
In the two cases, supposing that $E_F$ and $E_S$ are known, the determination of $H_F$ is possible, using a simple routine program applied to each couple of values for t and d. Basing their reasoning on the former model put forward by Burnett and Rickerby (1987a, 1987b), Ichimura et al. (2000) proposed an expression, which is a simplified form of eq. 19:

$$a = 3\left(\frac{t}{d}\right)\left(tg\xi\right)^{1/3}\left(\frac{H_F}{E_F}\right)^{1/2} \tag{20}$$

Another way to consider the problem was proposed by Korsunsky et al. (1998) who developed a model based on the work of indentation associated with the deformation energy of the two materials and their interface under the indent:

$$a = \frac{1}{1 + k_K \cdot \beta^2} \tag{21}$$

where β is the relative indentation depth (d/7t) and $k_K$ a fitting parameter. $H_F$ is determined by fitting the experimental values of $H_C$ in terms of β.
On the basis of geometrical considerations about the dimensions of the indent, Puchi-Cabrera (2002) proposed the computation of the composite hardness where two constants, $k_P$ and $n_P$, represent material parameters:

$$a = \exp\left(-k_P \cdot \beta^{n_P}\right) \tag{22}$$

The above-mentioned models express the composite hardness $H_C$ as a linear additive law in terms of the film and substrate hardness (eq. 16) comparable to a "series relation". Contrarily, Lesage et al. (2006) propose to consider a parallel relation:

$$\frac{1}{H_C} = \frac{1}{H_S} + a\left(\frac{1}{H_F} - \frac{1}{H_S}\right) \tag{23}$$

where the calculation of the film coefficient, a, is extensively described in Lesage et al. (2006). As an example, Chicot et al. (2008) studied the hardness of a TiN ceramic thin film (t = 1.1 μm) deposited on a stainless steel substrate (AISI 316L) by means of Magnetron Sputtering. Figure 6 shows the cross-section and the top view of the TiN film.

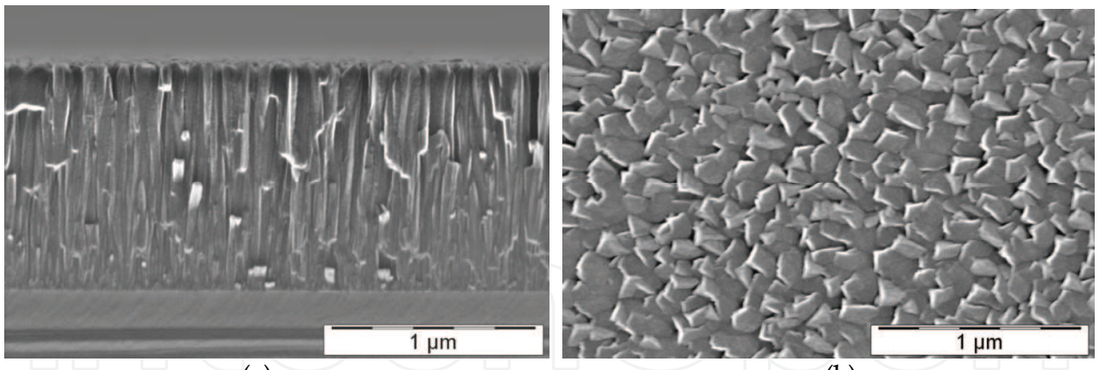


(a) (b)

Fig. 6. Cross-section (a) and in-plane-view (b) of the TiN film (SEM SE 20 kV 100000x) performed at ENEA in Brindisi.

In order to improve the accuracy of the film hardness determination, Chicot et al. (2008) employed three complementary approaches, i.e. Vickers hardness (HV) and Knoop hardness ($HK_P$) by using usual indentation tests (Table 1) and the contact hardness (HIT) deduced from load-depth curves analysis performed with a Vickers indenter (Table 2). Figure 7a represents the different hardness numbers as a function of the applied load on the same graph clearly showing disparities between the different techniques employed.

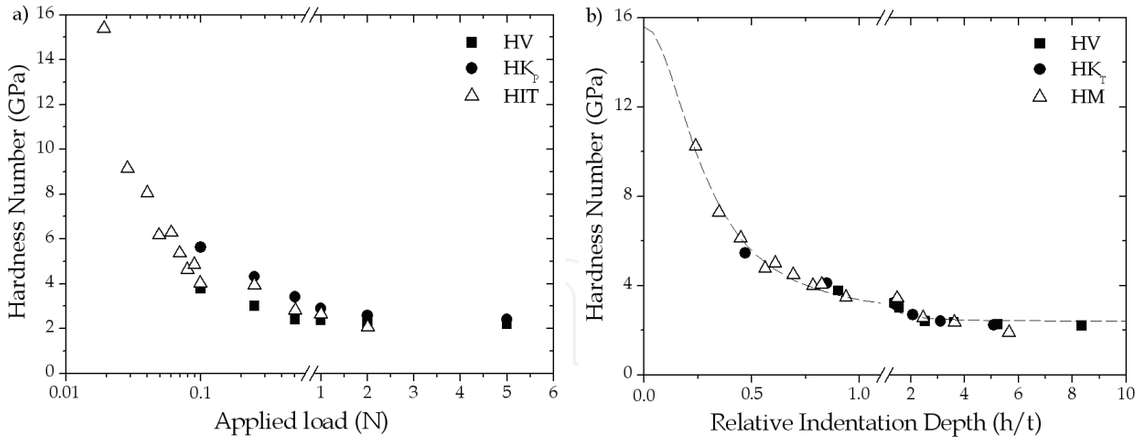


Fig. 7. (a) Hardness numbers from Vickers, Knoop and contact hardness calculations as a function of the applied load and (b) corrected hardness values as a function of the relative indentation depth.

In order to validly compare the indentation results obtained by the three methodologies, we converted Knoop hardness according to the eq. 4 and employed Martens hardness instead of HIT, which can vary to a great extent compared to Vickers or Martens hardness. As a result, Figure 7b shows that the consideration of the Vickers hardness, the Knoop hardness ($HK_T$) converted in an equivalent Vickers Hardness (eq. 4) and the Martens hardness (HM) allows the representation of all the hardness numbers as a function of the relative indentation depth on a unique curve. Finally, we have applied some thin film hardness models to determine the film hardness by using separately each set of hardness data. The macro-hardness of the film is collected in Table 4. Note that to give relevant prediction values; the model of Korsunsky requires indentation data for which the relative indentation depth is close to 0.1 thus explaining in this case that the predictive values are so low for Vickers and Knoop indentations.

| TiN, t = 1.1 µm | Models | Jönsson et al. (1984) | Chicot et al. (1995) | Korsunsky et al. (1998) | Lesage et al. (2006) |
|---|---|---|---|---|---|
| Hardness (GPa) | Vickers (HV) | 18.7 | 17.0 | 5.6 | 21.0 |
| | Knoop ($HK_T$) | 18.0 | 16.2 | 6.9 | 18.7 |
| | DSI (HM) | 18.8 | 16.8 | 16.3 | 17.4 |

Table 4. TiN ceramic thin film macro-hardness calculated by different film hardness models.

By analysing a loading curve performed on a thin film, it is possible to determine the ISE parameters of the film only by using eq. 15 to fit the part of the loading curve which is not affected by the substrate, i.e. for $h < t/10$. As an example, this fitting equation is applied on the loading curve obtained on the TiN thin film. Figure 8 shows the experimental load-depth curve obtained on the coated system and, as a reference, the substrate hardness also modelled by eq. 15.

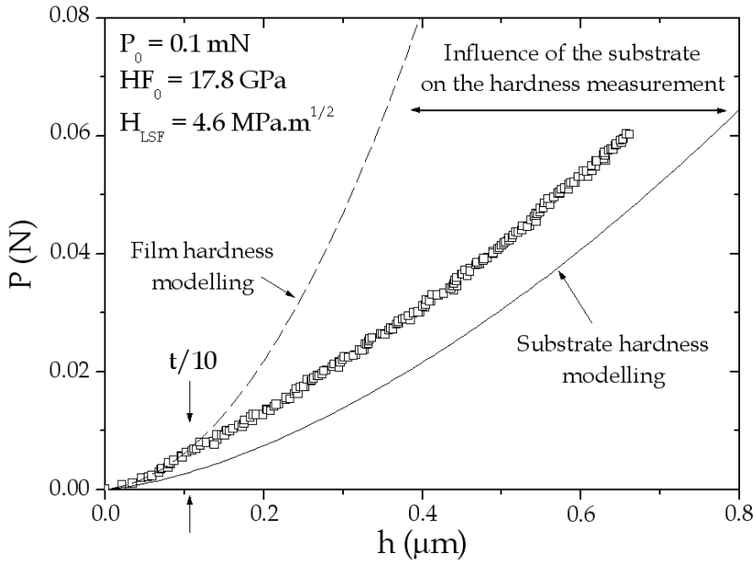


Fig. 8. Loading curve for the TiN thin film of 1.1 μm of thickness modelled by eq. 15.

It is clear that the measured hardness changes from the film hardness for lowest loads to the substrate hardness for highest loads. Then, by fitting the experimental data for which the indentation depth is lower than 10 % of the film thickness, i.e. 0.1 μm for t = 1.1 μm, we obtained the ISE parameters of the film as indicated in figure 8. The film macro-hardness obtained, i.e. 17.8 GPa, agrees very well with the hardness predicted values collected in Table 4. It is also clear that the accuracy of this methodology will depend on the range of hardness data available for applying the loading curve model.

## 3. Bulk modulus

### 3.1 Marshall's Method

The theoretical background for determining the bulk modulus of a material using the Knoop indentation test has been given by Marshall et al. (1980). The authors described a method for calculating the hardness/modulus ratio of a material from measurements of the Knoop indent diagonals. The decrease in the length of the indent diagonals is caused by elastic recovery of the material and, consequently, it can be related to the hardness/modulus ratio by the following equation:

$$\frac{w'}{L'} = \frac{w}{L} - \alpha \frac{HK_P}{E} \tag{24}$$

where w' and L' are the minor and the major diagonals of the measured Knoop indent. Contrarily, w and L are the minor and major diagonals of the ideal Knoop indent for which L/w equals to 7.11. $HK_P$ is the Knoop hardness calculated by the relation given in Table 1 and E is the bulk modulus. α is a constant equal to 0.45 (Marshall et al., 1980). Note that the major diagonal is not affected by the elastic recovery after the withdrawal of the indenter, then L' is equal to L. In addition, when considering the Knoop hardness $HK_T$ (Table 1), the coefficient α becomes equal to 0.5. Applied to the dense β-TCP ceramic (Fig. 9) using P = 5 N

and 10 indentation tests, we found 4.57 ± 0.12 GPa for $HK_P$ and 162.0 ± 26.5 GPa for the bulk modulus.

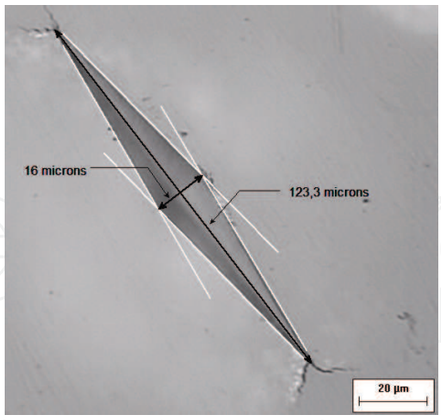


Fig. 9. Optical micrograph of a Knoop indentation performed on the dense β-TCP ceramic.

### 3.2 Oliver and Pharr method

Oliver and Pharr (1992) proposed that the bulk modulus could be calculated from the total compliance, $C_T = 1/S$ (Fig. 2b), of the specimen and of the instrument, which results from the contribution to the depth-measurement deflections of the load frame, added to the displacement into the material. Indeed, when load is applied, the reaction force is taken up by deflection of the load frame and it is this deflection that is typically added to the depth registration. The deflection is usually linearly proportional to the applied load in the manner of a linear spring (Fischer-Cripps, 2006). The correction takes the form of a product of the instrument compliance, $C_f$, and the load, P. This product must be subtracted from the depth recorded by the instrument:

$$h = h_{meas} - C_f \cdot P \tag{25}$$

where h and $h_{meas}$ are the sole indentation depth into the material and the measured indentation depth by the instrument, respectively.
Oliver and Pharr (1992), based on the original work of Doerner and Nix (1986), proposed the following relation:

$$\frac{1}{S} = \left(\frac{dh}{dP}\right) = C_t = C_f + \frac{\sqrt{\pi}}{2}\frac{1}{\beta \cdot \gamma \cdot E_R \sqrt{A_C}} \tag{26}$$

where $C_t$ is the total compliance, β is a correction factor which depends on the shape of the indenter and $A_C$ is the projected contact area of the elastic contact measured from the indentation hardness impression. $E_R$ is the reduced modulus defined as:

$$E_R = \left(\frac{1-\nu_m^2}{E_m} + \frac{1-\nu_i^2}{E_i}\right)^{-1} \tag{27}$$

where $E_m$, $\nu_m$ represent the bulk modulus and Poisson's ratio of the material and $E_i$, $\nu_i$ the elastic modulus and Poisson's ratio of the indenter, respectively.
The coefficient $\beta$ is considered as a pure geometric factor for indenters which are not described as bodies of revolution like the pyramidal square-based Vickers indenter. The correction factor $\beta$ is linked to the indenter geometry. King (1987) proposed a value of 1.012 for a Vickers indenter, whereas Dao et al. (2001) proposed a value of 1.07. Using a three dimension simulation of the Vickers indentation, Antunes et al. (2006) obtained 1.05 independently on the mechanical properties of the material. For a spherical indenter, the coefficient $\beta$ is equal to 1. Furthermore, to explain the overestimation of the elastic modulus calculated by application of eq. 26, Hay et al. (1999) pointed out that the assumptions in Sneddon's solution were overlooked, especially in the boundary conditions. Indeed, in Sneddon's solution for indentation of an elastic half-space by a rigid cone or a spherical indenter, radial inward displacements of surface points inside the circle of contact occur. To consider this effect, the authors introduced a complementary correction factor $\gamma$ in the eq. 26 which depends on the indenter shape.

### 3.3 Bulk modulus by Vickers and spherical indentations

The contact stiffness is very important in IIT since it is required to calibrate the indentation depth prior to the calculations. However, Chicot et al. (2009a and 2010b) have shown that it was not possible to calibrate the instrument prior to the bulk modulus calculation since the compliance value varies to a great extent as a function of the testing conditions; this phenomenon is also confirmed by Fischer-Cripps (2004). That is why in practice, we unfixed the compliance value and represented the contact stiffness as a function of the contact area according to eq. 26. For Vickers micro-indentation and by assuming a perfect contact area, i.e. by neglecting the top defect of the indenter, the projected contact area is then equal to:

$$A_C = 24.5 \cdot h_c^2 \tag{28}$$

By introducing eq. 28 into eq. 26, we obtained a linear relation between the inverse of the contact stiffness, (dh/dP), and the inverse of the contact indentation depth, $h_c$:

$$\left(\frac{dh}{dP}\right) = C_f + \sqrt{\frac{\pi}{24.5}} \frac{1}{2 \cdot (\beta\gamma) \cdot E_R} \cdot \frac{1}{h_c} \tag{29}$$

For Vickers indentation, the correction factor $\gamma$ introduced by Hay et al. (1999) is only Poisson's ratio dependent as follows:

$$\gamma = \pi \frac{\pi/4 + 0.1548 \cot\lambda (1-2\nu)\left[4(1-\nu)\right]^{-1}}{\left(\pi/2 - 0.8312 \cot\lambda (1-2\nu)\left[4(1-\nu)\right]^{-1}\right)^2} \tag{30}$$

where $\lambda$ (= 70.3°) is the semi-vertical angle of a conical indenter having the same area to depth ratio as the Vickers indenter (Veprek et al., 2006), i.e. $\pi \tan^2\lambda = 4\tan^2\xi$, where $\xi$ (68°) is the semi-angle between the two opposites faces of the pyramid.

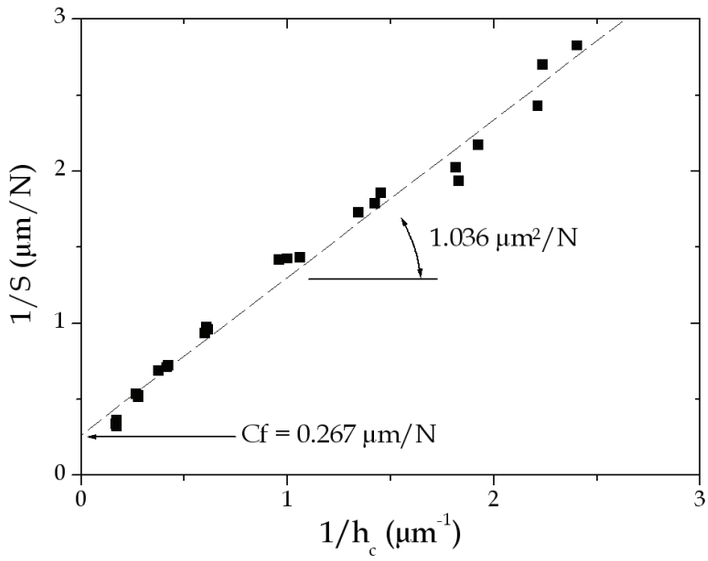


Fig. 10. 1/S as a function of $1/h_c$ for Vickers IIT performed on the dense β-TCP ceramic.

Figure 10 represents the inverse of the contact stiffness as a function of the inverse of the contact indentation depth obtained from Vickers indentation performed on the dense β-TCP ceramic. As a result, the representation is linear and therefore, the slope is directly linked to the bulk modulus of the material according to eq. 29. Then, by considering the elastic properties of diamond, i.e. 1140 GPa for the elastic modulus and 0.07 for the Poisson's ratio (Field and Telling, 1999) and by taking 0.3 for the Poisson's ratio of the material leading to 1.067 for the correction factor γ, the slope is reduced to $0.1598/E_R$. As a consequence, the reduced modulus is equal to 154.2 GPa and therefore, the bulk modulus of the dense β-TCP ceramic is equal to 162.1 ± 5.3 GPa. Note that this value is very close to the bulk modulus obtained by applying the Marshall's method.

For spherical indentation, Hertz's theory for sphere/plane contact provides three useful expressions:

1) The relation between the maximum indentation depth, $h_m$, and the contact indentation depth, $h_c$:

$$h_m = 2 \cdot h_c \tag{31}$$

2) The relation between the applied load, P, and the contact radius, $a_c$, where R is the spherical indenter radius:

$$P = \frac{4E_R a_c^3}{3R} \tag{32}$$

3) The relation between the total displacement and the contact radius:

$$h_m = \frac{a_c^2}{R} \tag{33}$$

By combining eq. 32 and eq. 33, we may write:

$$P = \frac{4}{3} E_R \sqrt{R}\, h_m^{3/2} \tag{34}$$

The derivation of the applied load compared to the maximum indentation depth leads to the following expression:

$$\frac{dP}{dh} = 2 E_R \sqrt{R}\, h_m^{1/2} \tag{35}$$

As a consequence, to take into account the frame compliance and relation 31 between $h_m$ and $h_c$, we expressed the inverse of the contact stiffness as a function of the square root of the contact indentation depth as follows:

$$\left(\frac{dh}{dP}\right) = C_f + \left(\frac{1}{2 \cdot \gamma \cdot E_R \cdot \sqrt{D}}\right) \frac{1}{\sqrt{h_c}} \tag{36}$$

where the correction factor γ, introduced by Hay et al. (1999) for a spherical indenter depends on the Poisson's ratio, the contact radius and the sphere indenter radius as follows:

$$\gamma = 1 + \frac{2(1-2\nu)}{3\pi(1-\nu)} \cdot \frac{a_c}{R} \tag{37}$$

Note that to be valid, eq. 31 must be verified. For the dense β-TCP ceramic, we plotted in figure 11 the contact indentation depth as a function of the maximum indentation depth.
Figure 11 shows a deviation compared to eq. 31, which occurs for the highest indentation depths associated to loads higher than 1 N. That is why the corresponding indentation data are not considered for the bulk modulus calculation. Figure 12 represents the inverse of the contact stiffness as a function of the contact indentation depth reciprocal in the case of spherical indentations.

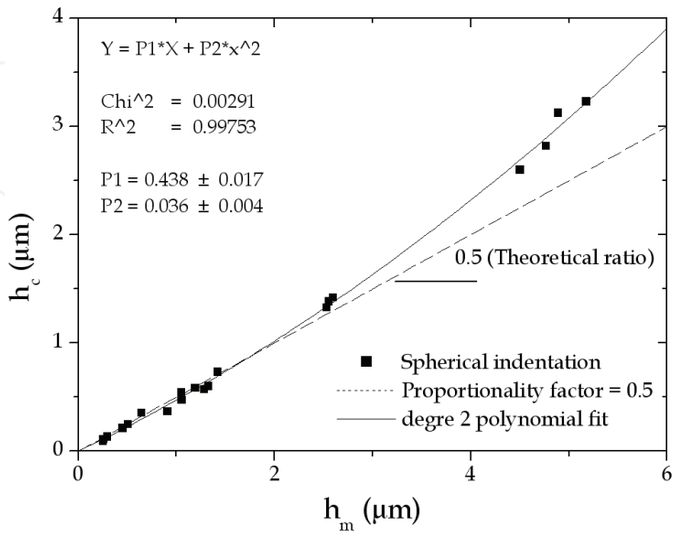


Fig. 11. $h_c$ versus $h_m$ for spherical indentation performed on the dense β-TCP ceramic.

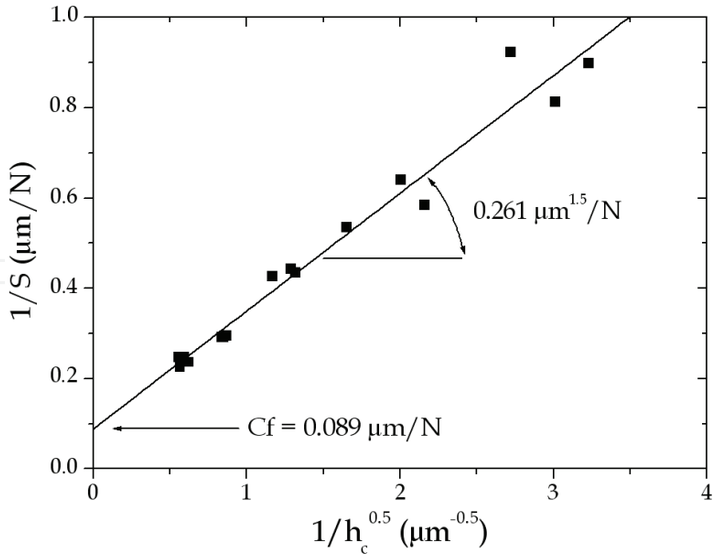


Fig. 12. 1/S as a function of $1/h_c^{0.5}$ for spherical IIT performed on the dense β-TCP ceramic.

Figure 12 confirms a linear variation that allows neglecting the correction factor, eq. 37, introduced by Hay et al. (1999) for spherical indentation which will lead to a non linear representation of the experimental data. The slope is proportional to the reduced modulus by $0.0354/E_R$ since the spherical indenter radius is equal to 100 µm. In this condition, the reduced modulus is equal to 135.6 GPa. By considering the elastic modulus and the Poisson's ratio of 540 GPa and 0.2 for the elastic properties of the tungsten carbide spherical indenter, the bulk modulus of the material is then equal to 162.6 ± 10 GPa, which is the same value found by Vickers indentation and by Marshall's method.

### 3.4 Bulk modulus of thin films

For a massive material, the inverse of the contact stiffness is a linear function of the inverse of the contact indentation depth obtained from Vickers indentation (Fig. 10), the corresponding slope being linked to the bulk modulus of the material. Then, instrumented indentation tests performed on a thin film would give a straight line when the substrate does not interfere with the measurement. On the contrary, the influence of the substrate is determined by two asymptotic limits corresponding to straight lines associated to the substrate behaviour for highest applied loads and to the film behaviour for the lowest applied loads, respectively. This phenomenon generally occurs for usual loads in micro-indentation and jointly for thin films. Figure 13 represents schematically the indentation results, which would be obtained from indentations performed on a hard film deposited onto a soft substrate.

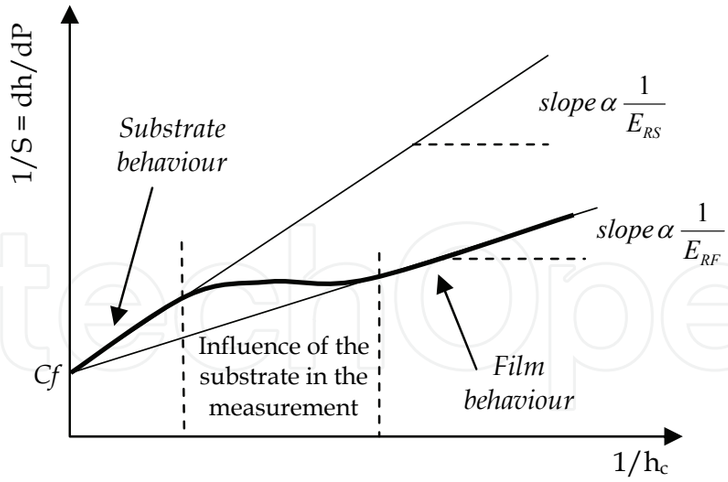


Fig. 13. Shematic representation of the contact stiffness variation of a coated system (hard film on soft substrate).

To represent correctly this behaviour, it is clear that an analytic model should consider the two limits, those of the film and of the substrate behaviours. The model proposed by Tricoteaux et al. (2010) is based on that of Korsunsky et al. (1998) initially developed for hardness measurement (eq. 21). Indeed, this model considers two asymptotic limits for the representation of the measured hardness of a coated material as a function of the relative indentation depth. Then, Tricoteaux et al. (2010) similarly suggested transposing eq. 16 devoted to hardness calculation, to the contact stiffness as follow:

$$\frac{1}{S_C} = \frac{1}{S_S} + a(h_c) \cdot \left( \frac{1}{S_F} - \frac{1}{S_S} \right) \tag{38}$$

where $S_C$, $S_S$ and $S_F$ are the contact stiffness corresponding to the *composite* material (substrate + film), the substrate and the film respectively. $a(h_c)$ represents the film contribution which depends on the contact depth.
By combining eq. 21, eq. 26 and eq. 38, we obtained the following expression for determining the bulk modulus of the film:

$$\frac{1}{S_C} = C_f + \left( \frac{1}{2\beta} \sqrt{\frac{\pi}{24.5}} \frac{1}{\gamma_S E_{RS}} \right) \frac{1}{h_c} + \frac{1}{h_c} \left( \frac{1}{1 + \frac{k}{t^2} h_c^2} \right) \left( \frac{1}{2\beta} \sqrt{\frac{\pi}{24.5}} \right) \left( \frac{1}{\gamma_F E_{RF}} - \frac{1}{\gamma_S E_{RS}} \right) \tag{39}$$

where $E_{RF}$ and $E_{RS}$ are defined according to the relation (27) for the film and the substrate, respectively.
From a general point of view, eq. 39 can be simply presented as follows, where the coefficients Pi are fitting parameters allowing the determination of the elastic properties:

$$\frac{1}{S_C} = P_1 + \frac{P_2}{h_c} + \frac{P_3}{h_c\left(1 + P_4 h_c^2\right)} \tag{40}$$

By comparing eq. 40 to eq. 39, we observed that the parameter $P_2$ only depends on the bulk modulus of the substrate, whereas $P_3$ depends on both substrate modulus and film modulus. As an example, the model is applied on TiCN PECVD thin films with film thickness of 2.2 µm deposited on a stainless steel substrate. Figure 14 shows a very good fit of the experimental data with a correlation coefficient $R^2$ very close to 1.

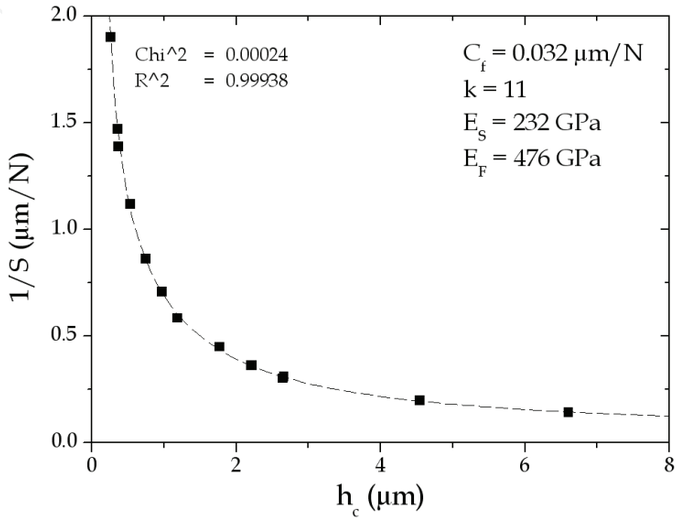


Fig. 14. Model for bulk modulus calculation of thin film applied to a TiCN thin film of 2.2 µm in thickness.

From the fitting parameters, the calculated value of the bulk modulus of the film is equal to 476 GPa in agreement with the values given by Karlsson et al. (2000) for similar coatings. Note that the bulk modulus of the substrate can be considered as unknown parameters. In this case, the model has been applied and the bulk modulus deduced from $P_2$ has been found to be equal to 232 GPa, which is a reasonable value.

## 4. Tensile mechanical properties

The true-stress and true-strain determined by uniaxial tensile tests are equivalent to spherical indentation stress and strain through the following expressions (Herbert et al., 2001):

$$\sigma_{\text{indentation}} \approx \frac{p_m}{3} \approx \sigma_{\text{uniaxial tension}} = \sigma \tag{41}$$

$$\varepsilon_{\text{indentation}} \approx 0.2\frac{a_c}{R} \approx \varepsilon_{\text{uniaxial tension}} = \varepsilon \tag{42}$$

where $p_m$ is the mean pressure equivalent to the Meyer hardness calculated for spherical indentation, $a_c$ is the contact radius and R the nominal radius of the indenter. Note that the ratio is sometimes taken equal to 2.8.
The mean pressure is calculated by:

$$p_m = \frac{P}{\pi \cdot a_c^2} \tag{43}$$

It is important to note that eq. 41 and eq. 42 are applicable in the limit of a fully developed plastic contact, i.e. when $a_c/R$ is close to 0.16 independently of the magnitude of the non-dimensional parameter $\sigma_y/E$ and the Poisson's ratio of the material. Moreover, in order to represent the plastic domain in tensile stress-strain deformation, different relations can be employed (Hollomon, 1945; Swift, 1952; Ludwik, 1909), the Hollomon's law being probably the most used:

$$\sigma = K_H \cdot \varepsilon^{n_H} \tag{44}$$

where $K_H$ and $n_H$ are the strength coefficient and the strain-hardening exponent, respectively.
In order to be valid, the stress expressed in eq. 44 must be calculated considering the plastic strain. In practice when Hollomon's law is not verified, the Ludwik's law is preferred to the Swift's law:

$$\sigma = \sigma_y + K_L \cdot \varepsilon^{n_L} \tag{45}$$

where $K_L$ and $n_L$ are the strength coefficient and the strain-hardening exponent, corresponding to this law, respectively.
From Hollomon's law, Alcala et al. (2000) combined equations (42), (43) and (44) to write:

$$p_m = 2.8 K_H \cdot \left(0.2 \frac{a_c}{R}\right)^{n_H} \tag{46}$$

Matthews (1980) by analyzing work-hardening materials following eq. 43 and eq. 44 provided an alternative expression for the mean contact pressure, $p_m$:

$$p_m = \frac{6 \cdot K_H}{(2 + n_H)} \cdot \left(\frac{8 \cdot a_c}{9\pi \cdot R}\right)^{n_H} \tag{47}$$

Based on the Ludwik's law, Huang et al. (2007) suggested representing the mean pressure as the function of the flow stress, $\sigma_{flow}$, and taking into account the indentation size effect as follows:

$$p_m = 2.8 \cdot \sigma_{flow} = 2.8 \cdot \sigma_{ref} \cdot \sqrt{\left[f(\varepsilon)\right]^2 + \frac{\ell}{R}} \tag{48}$$

where $\ell$ represents the ISE in spherical indentation. The stress, $\sigma_{ref}$, and the function, f, are deduced from Ludwik's law as follows:

$$\sigma = K_L\left(\frac{\sigma_y}{K_L} + \varepsilon^{n_L}\right) = \sigma_{ref}\cdot f(\varepsilon) \tag{49}$$

Then, by combining relations (42), (48) and (49), it is possible to express the applied load as a function of the indentation depth over the entire loading curve:

$$p_m = 2.8\cdot K_L\cdot\left(\sqrt{\left[\left(\frac{\sigma_y}{K_L}\right)+\left(0.2\frac{a_c}{R}\right)^{n_L}\right]^2+\frac{\ell}{R}}\right) \tag{50}$$

On the other hand, Gao (2006) proposed the introduction of strain-hardening and indentation size effect for conical and spherical indentation tests in the expanding cavity models (ECMs). The author expressed the ratio between the mean pressure, $p_m$, and the yield stress, $\sigma_y$, as a function of the contact radius to the indenter tip radius ratio. The proposed relations depend on the mechanical behaviour of the tested material and on the shape of the indenter.
Then, for spherical indentation, the relations are:
- For elastic perfectly plastic when no strain gradient effect is considered,

$$\frac{p_m}{\sigma_y} = \frac{2}{3}\cdot\left[\frac{7}{4}+\ln\left(\frac{1}{4}\frac{E}{\sigma_y}\frac{a_c}{R}\right)\right] \tag{51}$$

- For elastic perfectly plastic with strain gradient effect, factor c,

$$\frac{p_m}{\sigma_y} = \frac{2}{3}\cdot\left[\frac{7}{4}+\ln\left(\frac{1}{4}\frac{E}{\sigma_y}\frac{a_c}{R}\right)\right]-\frac{12c}{5E}\left[\left(\frac{9}{16}\frac{E}{\sigma_y}\frac{a_c}{R}\right)-\left(\frac{1}{4}\frac{E}{\sigma_y}\frac{a_c}{R}\right)^{-2/3}\right]\cdot\frac{1}{a_c^2} \tag{52}$$

- For elastic strain-hardening when no strain gradient effect is considered,

$$\frac{p_m}{\sigma_y} = \frac{2}{3}\cdot\left\{1+\frac{3}{4}\left(\frac{1}{4}\frac{E}{\sigma_y}\frac{a_c}{R}\right)^{n_H}+\frac{1}{n_H}\left[\left(\frac{1}{4}\frac{E}{\sigma_y}\frac{a_c}{R}\right)^{n_H}-1\right]\right\} \tag{53}$$

- For elastic strain-hardening with strain gradient effect, factor c,

$$\frac{p_m}{\sigma_y}=\frac{2}{3}+\frac{1}{2}\left(\frac{1}{4}\frac{E}{\sigma_y}\frac{a_c}{R}\right)^{n_H}+\frac{2}{3\,n_H}\left[\left(\frac{1}{4}\frac{E}{\sigma_y}\frac{a_c}{R}\right)^{n_H}-1\right]-\frac{12c}{5E}\cdot\left[\left(\frac{9}{16}\frac{E}{\sigma_y}\frac{a_c}{R}\right)-\left(\frac{1}{4}\frac{E}{\sigma_y}\frac{a_c}{R}\right)^{-2/3}\right]\cdot\frac{1}{a_c^2} \quad (54)$$

And for Vickers indentations where λ is defined in eq. 30, the relations are deduced from those for conical indentations:

- For elastic perfectly plastic when no strain gradient effect is considered,

$$\frac{P}{24.5\cdot\sigma_y}=\frac{2}{3}\cdot\left[\frac{7}{4}+\ln\left(\frac{1}{3}\frac{E}{\sigma_y}\cot\lambda\right)\right]\cdot h^2 \quad (55)$$

- For elastic perfectly plastic with strain gradient effect,

$$\frac{P}{24.5\cdot\sigma_y}=\frac{2}{3}\cdot\left[\frac{7}{4}+\ln\left(\frac{1}{3}\frac{E}{\sigma_y}\cot\lambda\right)\right]\cdot h^2-\frac{12c}{5E}\cdot\left(\frac{\pi\tan\lambda}{24.5}\right)^2\cdot\left[\left(\frac{3}{4}\frac{E}{\sigma_y}\cot\lambda\right)-\left(\frac{1}{3}\frac{E}{\sigma_y}\cot\lambda\right)^{-2/3}\right] \quad (56)$$

- For elastic strain-hardening when no strain gradient effect is considered,

$$\frac{P}{24.5\cdot\sigma_y}=\frac{2}{3}\cdot\left\{1+\frac{3}{4}\left(\frac{1}{3}\frac{E}{\sigma_y}\cot\lambda\right)^{n_H}+\frac{1}{n_H}\left[\left(\frac{1}{3}\frac{E}{\sigma_y}\cot\lambda\right)^{n_H}-1\right]\right\}\cdot h^2 \quad (57)$$

- For elastic strain-hardening with strain gradient effect,

$$\frac{P}{24.5\cdot\sigma_y}=\left\{\frac{2}{3}+\frac{1}{2}\left(\frac{1}{3}\frac{E}{\sigma_y}\cot\lambda\right)^{n_H}+\frac{2}{3n_H}\left[\left(\frac{1}{3}\frac{E}{\sigma_y}\cot\lambda\right)^{n_H}-1\right]\right\}\cdot h^2-\frac{12c}{5E}\cdot\left(\frac{\pi\tan\lambda}{24.5}\right)^2\cdot\left[\left(\frac{3}{4}\frac{E}{\sigma_y}\cot\lambda\right)-\left(\frac{1}{3}\frac{E}{\sigma_y}\cot\lambda\right)^{-2/3}\right] \quad (58)$$

Note that relations (55) to (58) correspond to the extended relations (9) and (12). Then, the second terms in eq. 56 and eq. 58 can be also associated with the zero shift $P_0$ in eq. 12. Independently of that, the determination of the tensile mechanical properties without any prior information on the mechanical behaviour of the material can be obtained by fitting these relations, allowing the determination of the yield stress, $\sigma_y$, strength coefficient, $K_H$ or $K_L$, strain-hardening exponent, $n_H$ or $n_L$, elastic modulus, E, and the constants, c or $\ell$, characterizing the indentation size effect or the zero shift. A discussion about the value of these parameters must be helpful for identifying the mechanical behaviour of the material.

As an example, for studying the mechanical behaviour of the dense β-TCP ceramic, we plotted the indentation stress-strain data (Fig. 15) where the mean pressure under a sphere to plane contact is calculated by applying relation (43) and the ratio ($a_c$/R) is calculated from eq. 33, where $h_m$ represents the indentation depth reached during the indentation test. In addition by combining eq. 32 and eq. 43, we may express the mean pressure as a function of the ratio ($a_c$/R) as follows:

$$P_m = \frac{4E_R}{3\pi}\frac{a_c}{R} \text{ with } \frac{a_C}{R} = \sqrt{\frac{h_m}{R}} \quad (59)$$

By taking into account the reduced modulus of the dense β-TCP ceramic equal to 135.5 GPa for spherical indentation (see part 3.3), we plot eq. 59 in figure 15 where the dash straight line corresponds to the theoretical Hertzian elastic response. As it is clearly seen, the Hertzian theory is verified until a limit value, $p_y$, which corresponds to the yield indentation stress as earlier demonstrated by Zhu et al. (2008).

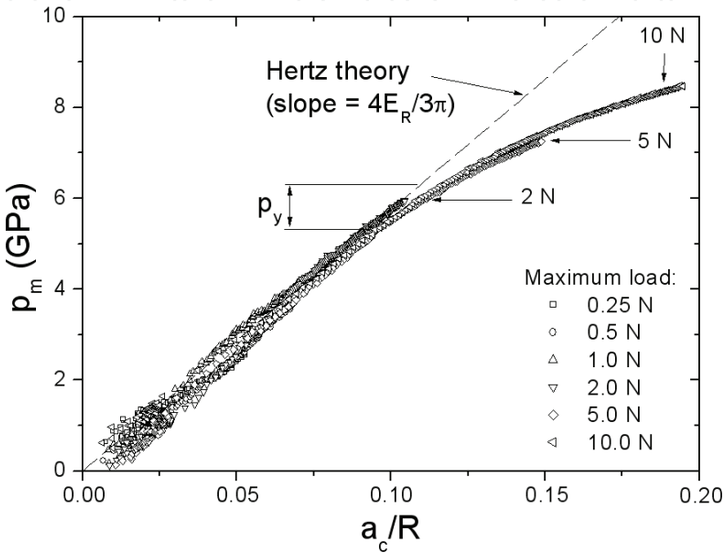


Fig. 15. Indentation stress-strain curve deduced from spherical IIT performed on the dense β-TCP ceramic.

For modelling the plastic domain of the dense β-TCP ceramic, we consider the indentation data drawn from spherical indentations for which the applied loads give a mean pressure higher than 5.5 GPa that seems to be the limit, $p_y$, between elastic and plastic domains as shown in figure 15. Without any information about the mechanical behaviour of such a ceramic, we applied the models of Alcala et al. (2000), Matthews (1980) and Huang et al. (2007) and the expanding cavity models developed for elastic perfectly plastic materials and for elastic strain-hardening materials by Gao (2006). Table 5 collects the values of the mechanical parameters according to the tested models.

| | Spherical indentations | | | | | | | Vickers indentations | | | |
|---|---|---|---|---|---|---|---|---|---|---|---|
| Eq. n° | (46) | (47) | (50) | (51) | (52) | (53) | (54) | (55) | (56) | (57) | (58) |
| $K_H$, $K_L$ (GPa) | 21.7 | 21.4 | 7.4 | - | - | - | - | - | - | - | - |
| $n_H$, $n_L$ | 0.60 | 0.60 | 0.18 | - | - | - 0.60 | - 0.65 | - | - | 0.14 | 0.16 |
| $\sigma_y$ (GPa) | - | - | 1.8 | 6.6 | 6.0 | 8.2 | 8.3 | 2.1 | 2.2 | 1.8 | 1.8 |
| E (GPa) | - | - | - | 165 | 159 | 122 | 118 | 162 | 157 | 155 | 135 |
| $\ell$ (μm) | - | - | -0.047 | - | - | - | - | - | - | - | - |
| c (N) | - | - | - | - | - 0.95 | - | 0.03 | - | 0.03 | - | 0.03 |

Table 5. Tensile mechanical properties deduced from the different models applied to spherical and Vickers IIT performed on the dense β-TCP ceramic.

It is noticeable that the models of Alcala et al. (2000), eq. 46, and Matthews (1980), eq. 47, give the same values for the strain-hardening exponent, $n_H$, and for the strength coefficient, $K_H$, which lead to the same representative curve in figure 16a. Contrarily, the model of Huang et al. (2007) allows a better fit of the experimental data (Fig. 16a) but gives very different parameters since it considers the Ludwik's law instead of the Hollomon's law.

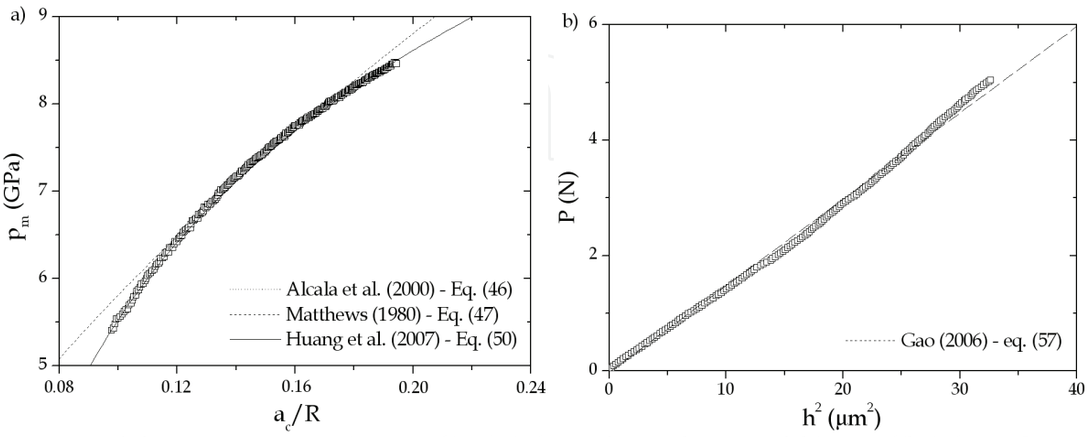


Fig. 16. Models representing a) $p_m = f(a_c/R)$ for spherical IIT and b) $P = f(h^2)$ for ECM and Vickers IIT performed on the dense β-TCP ceramic.

On the other hand, even if the expanding cavity models are able to adequately represent the experimental data, some values indicated in table 5 have no physical meaning such as the negative value for the work-hardening exponent. In the other cases of ECMs, the bulk modulus is in a good agreement with the theoretical value. Additionally, it can be seen that the introduction of the ISE has no significant influence on the values of the tensile parameters. For ECMs, eq. 55 to eq. 58, the bulk modulus is close to 160 GPa as already found by spherical indentations. However, the yield stress is three times less but of the same order of magnitude than the value found by the model of Huang et al. (2007). This difference has been observed by Zhu et al. (2008) who have highlighted the influence of the spherical indenter radius on the yield indentation stress. On the other hand, it is very interesting to note that the coefficients in the Ludwik's law deduced from the application of the model of Huang et al. (2007), eq. 50, are the same than those obtained by the expanding cavity model in the case of an elastic strain-hardening behaviour by considering or not the indentation size effect in the ECM developed for Vickers indentation, as shown in figure 16b. As a result, we can conclude that the tensile mechanical properties of the dense β-TCP ceramic in the non elastic domain can be modelled by Ludwik's law as follows, when the stress is expressed in GPa:

$$\sigma = 1.8 + 7.4 \cdot \varepsilon^{0.18} \tag{60}$$

## 5. Vickers Indentation Fracture Toughness

The Vickers indentation test is often used for determining the fracture toughness of ceramics. This method consists in indenting the ceramic with a Vickers indenter in order to generate cracks at the extremities of the indent. Afterwards, the toughness is calculated from the

dimensions of the indent diagonals and of the crack lengths. Since the Vickers Indentation Fracture (VIF) test is not standard, the calculated value for the toughness is called Kc instead of KIc. In practice, it is generally admitted that the cracks can be developed following radial-median or Palmqvist modes as represented in figure 17.

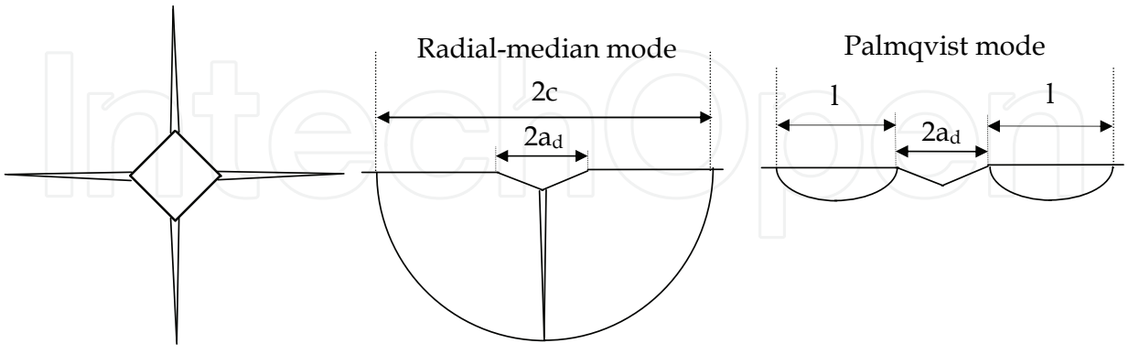


Fig. 17. Schematic representation of Vickers indentation cracks according to radial-median and Palmqvist modes.

The Vickers Indentation Fracture toughness can be calculated from various relationships depending on the load, indent diagonal, cracks length and Young's modulus to hardness ratio. Ponton & Rawlings (1989) have collected close to 20 crack equations depending on the cracking mode. More recently, Chicot et al. (2009b) have compared these relations and proposed to consider the average relations as follows according to the cracking mode:

$$\text{For Radial-median cracks: } Kc_{(R-M)} = 0.0154 \cdot \left(\frac{E}{HV}\right)^{1/2} \cdot \frac{P}{c^{3/2}} \tag{61}$$

$$\text{For Palmqvist cracks: } Kc_{(P)} = 0.0089 \cdot \left(\frac{E}{HV}\right)^{2/5} \cdot \frac{P}{a_d l^{1/2}} \tag{62}$$

Obviously, Kc must be an intrinsic parameter of the material, then the ratios ($P/c^{3/2}$) and ($P/a_d l^{1/2}$) of eq. 61 and eq. 62 should be constant independently of the applied load. In addition, eq. 62 is connected to the indent half diagonal, $a_d$, which is load dependent due to the indentation size effect. The simplest mathematical relation between the half-diagonal $a_d$ and the load P is given by the Meyer's law (1908) (Table 3). By introducing Meyer's law into eq. 62, we may write the two following proportionality relations:

$$\text{For Radial-median cracks: } c \propto P^{2/3} \tag{63}$$

$$\text{For Palmqvist cracks: } l \propto P^{2\left(1-\frac{1}{n}\right)} \tag{64}$$

Then the cracking mode can be identified by comparing the experimental slope of ln c = f (ln P) to 2/3 or the experimental slope of ln l = f (ln P) to 2(1 – 1/n) for Radial-median and Palmqvist cracking modes, respectively.
However, in some cases, neither of these proportionality relations is verified because the cracking mechanism does not correspond to the usual cracking modes but to an intermediate state. Based on the cracking toughness relations from Miranzo et al. (1984) and on the work of Chicot et al. (2009b), we suggest the following expression to calculate VIF toughness for an intermediate cracking mode:

$$Kc_{(I-M)} = (\alpha - \beta \cdot q) \cdot f\left(\frac{E}{HV}\right) \cdot \frac{P}{a_d^q c^{(1.5-q)}} \tag{65}$$

where α and β are constants depending on the material, q is a constant ranging between 0 and 1 that describes the intermediate cracking mode and f(E/Hv) is a function which depends on the Young's modulus and the Vickers hardness as follows:

$$f\left(\frac{E}{HV}\right) = \frac{\left[\beta_{exp}^2 / \delta\right] - 1.5}{0.75} \text{ with } \delta = \frac{2}{3} \cdot \left(1 + \ln \beta_{exp}\right) \text{ and } \beta_{exp} = 0.768 \cdot \left(\frac{E}{HV}\right)^{0.408} \tag{66}$$

The two constants α and β are calculated by considering the two limit conditions for eq. 65. Indeed, when q = 0, $Kc_{(I-M)}$ corresponds to the Radial-median cracking mode (eq. 61) and when q = 1, $Kc_{(I-M)}$ corresponds to the Palmqvist cracking mode (eq. 62). Afterwards the exponent q is calculated from the following relation:

$$q = \left(\frac{1.5 \cdot s - 1}{s}\right) \cdot n \tag{67}$$

where s corresponds to the experimental slope of ln c = f (ln P) and n to the Meyer's index.
This methodology is applied on annealed bioglass (55 $SiO_2$ - 13.5 CaO - 31.5 $Na_2O$). However, as shown on Figure 18 for this type of very brittle materials, a secondary crack network appears in the vicinity of the four indent edges in addition to the main cracks generated at the four indent extremities. According to Roman et al. (2002), a mean crack length corresponding to an equivalent four cracks network is calculated by dividing the total cracks length by four.

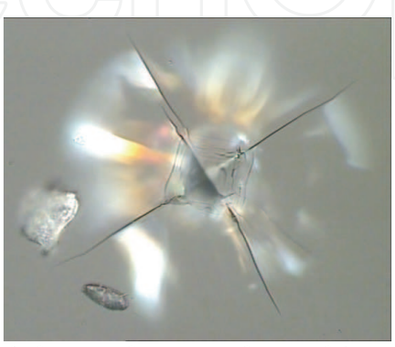

Fig. 18. Optical micrograph of the crack network resulting from Vickers indentation test performed on the (55 $SiO_2$ - 13.5 CaO - 31.5 $Na_2O$) bioglass.

For this bioglass, the Young's modulus and the Vickers hardness are equal to 63.6 GPa and 5.15 GPa, respectively and Meyer's index n is equal to 1.88. Figure 19 shows that cracking corresponds to an intermediate mode. Indeed, the slope s of ln c = f (ln P) is equal to 0.815, very different to the theoretical value 2/3 for a radial-median cracking mode. Moreover, the slope of ln l = f (ln P) is experimentally equal to 1.068, which is also different of the theoretical value 2(1-1/n) = 0.936 calculated from the Meyer's index (eq. 64) for a Palmqvist cracking mode. As a result, the exponent q calculated from eq. 67 is equal to 0.78 which is an intermediate value between 0 (Radial-median) and 1 (Palmqvist), the constants $\alpha$ and $\beta$ in eq. 66 are equal to 0.0169 and 0.0065, respectively, found by equating the toughness calculation to the two limits. The VIF toughness Kc is found equal to 1 MPa.m$^{1/2}$, which is very close to the toughness measured by Rajendran et al. (2002) on $SiO_2$-CaO-$Na_2O$-$P_2O_5$ bioglasses.

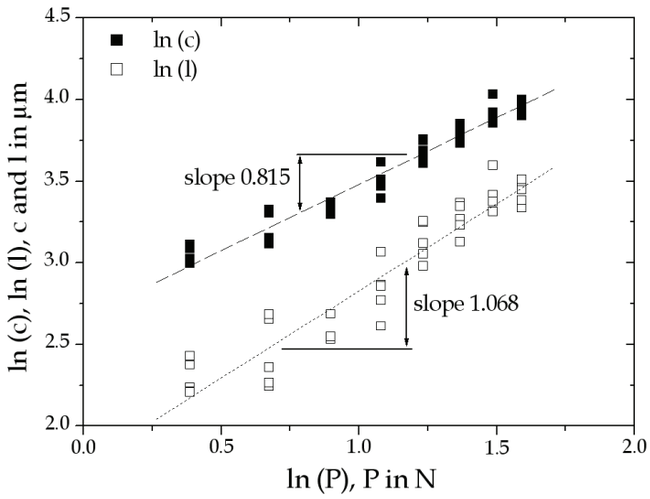


Fig. 19. Crack length criterion applied to results obtained on a $SiO_2$-CaO-$Na_2O$ bioglass.

## 6. Adhesive properties of ceramic coatings

### 6.1 Scratch test

Heavens (1950), was the first to propose that the scratch test could be used for a qualitative evaluation of coating adhesion. Later, Benjamin and Weaver (1960) presented the first analysis by this test and proposed a model to connect the critical applied load, Lc, with the mechanical properties of the substrate and the adhesion of the coating. After, the scratch test has been used extensively for adhesion characterization of hard coatings such as TiN or TiC on steel (Laeng and Steinmann, 1981; Perry et al., 1981; Mittal, 1987). Generally, a Rockwell diamond tip is moved on the film at a constant velocity while a constant normal force (Laeng and Steinmann, 1981) or an increasing normal force is applied with a constant loading rate (Steinmann et al., 1987). During the indentation scratch test, the indenter introduces stresses at the interface between film and substrate causing delamination or chipping of the film. The adhesive property is then represented by the critical load at which the failure of the film is detected. The film failure characterized by the critical load, $L_C$, can be determined by the change in friction or in acoustic emission, or by observation of the scratch track. Moreover, the intensity of the acoustic emission depends on the type of film failure during the adhesion test e.g. cracking, chipping (cohesive failure) and delamination

(adhesive failure). The scratch test often uses an optical microscope to confirm the critical load. Nevertheless, it is often difficult to identify representative damage of interfacial decohesion and mechanical origins of damages. In addition, Sekler et al. (1988) discussed widely about the different techniques for determining the critical load of coated systems (microscopy, acoustic emission, and normal, tangential and lateral forces). In addition to the $L_C$ calculation, Benayoun et al. (1999) presented different expressions for the film/substrate adhesion energy. Indeed, the expression for the critical shearing, $\tau_C$, given by Benjamin and Weaver (1960), Weaver (1975) and Perry et al. (1981) is:

$$\tau_C = kH \cdot \left(\frac{d_C}{2R}\right) \cdot \left[1 - \left(\frac{d_C}{2R}\right)^2\right]^{-0.5} \tag{68}$$

where H is the hardness of the sample, $d_C$ the scratch track width obtained at the critical load and R the tip radius of the indenter. k a numerical coefficient between 0.2 and 1.
Felder and Laugier (1992) proposed a similar expression:

$$\tau_C = p_m \cdot \left(\frac{d_C}{2R}\right) \text{ with } p_m = \frac{8L_C}{\pi d_C^2} \tag{69}$$

where $p_m$ is the mean indentation pressure for a given critical load $L_C$.
As an example, figure 20 shows the results of an indentation scratch test obtained for a progressive load scratch (0.1 – 15 mN) on a polymer topcoat. This figure representing penetration depth (Pd), residual depth (Rd) and normal load during post-scan (FnP) signals clearly shows the critical load ($L_C1$) which corresponds exactly to the fracture point on the optical micrograph (CSM Bulletin, 2008).

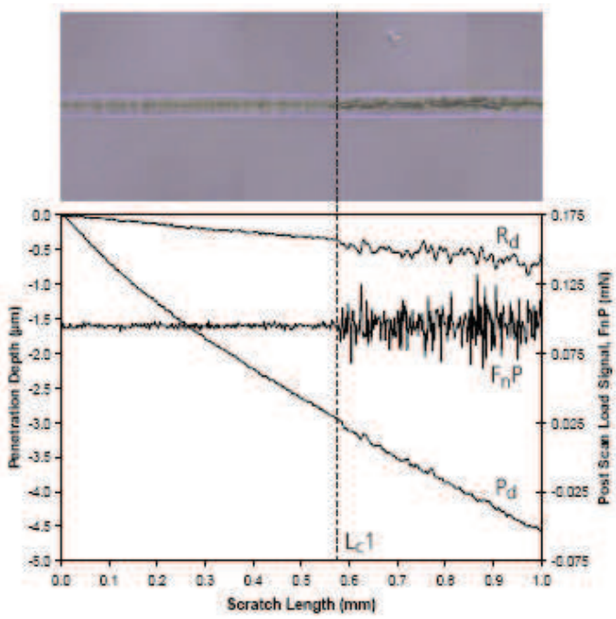


Fig. 20. Scratch test results for a progressive load scratch (0.1 – 15 mN) on a polymer topcoat.

### 6.2 Interface Indentation Test

Vickers indentation tests performed at the interface between a thick coating and its substrate can create and propagate a crack located in the plane of the interface, as it can be seen in figure 21 (Chicot et al., 1996).

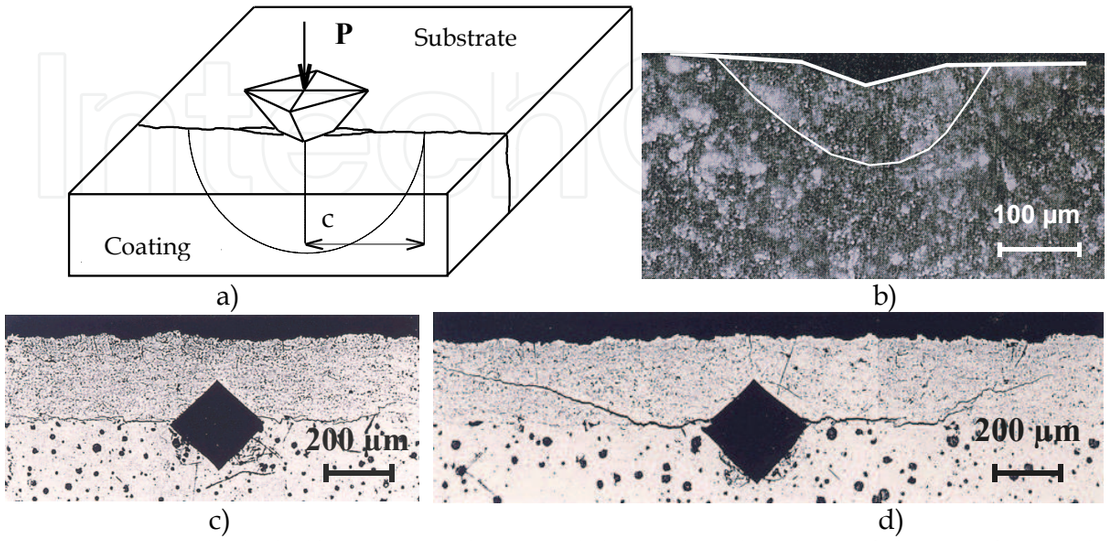


Fig. 21. a) Principle, b) half-penny crack, c) crack located in the plane of the interface and d) deviation of the crack towards the coating. The Vickers indentation test was performed at the interface of a $Cr_3C_2$/NiCr coating deposited on low carbon steel.

The test consists in measuring the crack lengths as a function of the applied load and to calculate the apparent interface toughness using an expression resulting from the analysis of different models developed for determining toughness of brittle massive materials by indentation. For the interfacial indentation, it was emphasized that the indented material, composed of substrate, coating and interface itself, can be considered as a unique brittle material (Chicot et al., 1996). The methodology is the following:

1) Obtaining a polished cross-section of the coated sample, in order to perform Vickers indentation tests with different applied loads, for which the indent diagonal must be coincident with the coating/substrate interface;
2) For each indentation test, measuring the value of the half indent diagonal (d/2) and the crack length (c), both at the interface;
3) Plotting these data as a function of the applied load in bi-logarithmic scale, as represented schematically in figure 22; where d/2 = f (P) is called "apparent hardness" and c = f (P) the cracking line;
4) Determining the coordinates of the critical point, ($P_C$, $c_c$) in figure 22, underneath which no cracking is observed at the interface and which are used to compute the apparent interface toughness of the coating/substrate couple.

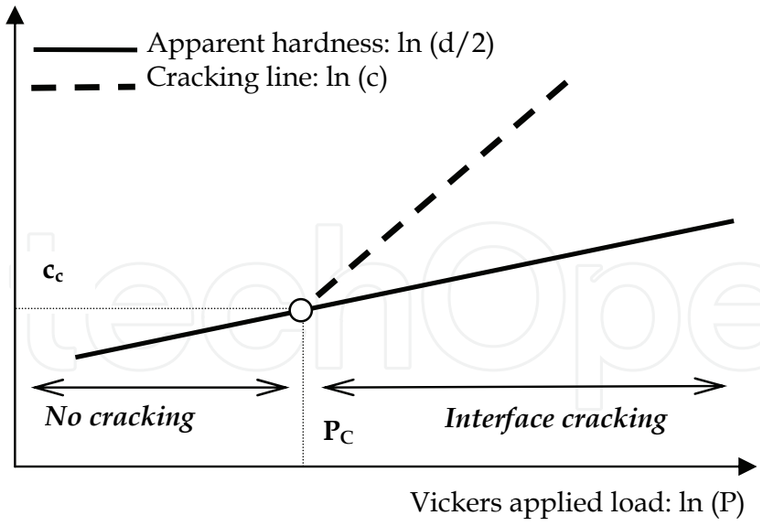


Fig. 22. Schematic representation of the apparent hardness, the cracking line and the critical point used to calculate the apparent interface toughness.

During indentation, a plastic deformation zone is created by sharing the combined local properties of the coating and of the substrate. Eventually, a local crack may be likely to occur in the interface plane if the fracture toughness of this composite interface material is attained. The purpose of the interface indentation test is to give a quantitative measurement of the apparent fracture toughness. Some general formulations found in the literature involve a ratio between elastic modulus and hardness of the material. For the interface material, Chicot et al. (1996) proposed to express this parameter as the square root of the ratio of the elastic modulus (E) divided by the Vickers hardness (HV) at the interface, by considering the mean geometrical features of the substrate and coating couple:

$$\left(\frac{E}{HV}\right)_i^{1/2} = \frac{\left(\frac{E}{HV}\right)_S^{1/2}}{1+\left(\frac{HV_S}{HV_C}\right)^{1/2}} + \frac{\left(\frac{E}{HV}\right)_C^{1/2}}{1+\left(\frac{HV_C}{HV_S}\right)^{1/2}} \tag{70}$$

where the subscripts i, S and C stand for interface, substrate and coating, respectively.
Then, by connecting the critical load used to initiate a crack, $P_c$, and the corresponding half-indent diagonal, $c_c$, we propose to calculate the apparent interface toughness representing the adhesion of the coating on its substrate by the following relation, in a similar way than those proposed earlier for bulk materials by Lawn et al. (1980) or Anstis et al. (1981) presented as the eq. 61:

$$Kca = 0.0154 \cdot \frac{P_c}{c_c^{3/2}} \cdot \left(\frac{E}{HV}\right)_i^{1/2} \tag{71}$$

Although this relation is only valid for cracks that are longer than the plastic zone radius, it was emphasized that the crack line can be extrapolated at the critical point. Then, the couple ($P_C$, $c_C$) can be used for the calculation of an apparent interface toughness, Kca. The critical point is chosen because when a crack is formed, its propagation is aided by the bending of the coating due to the action of the indenter, which plays the role of a wedge inserted at the interface. Consequently the propagation depends on the coating thickness since a thicker coating will resist to the bending better than a thinner one. Therefore, the slope of the cracking line is affected by the elastic behaviour of the coating. The only point which is not concerned is the crack initiation point, ($P_C$, $c_C$).

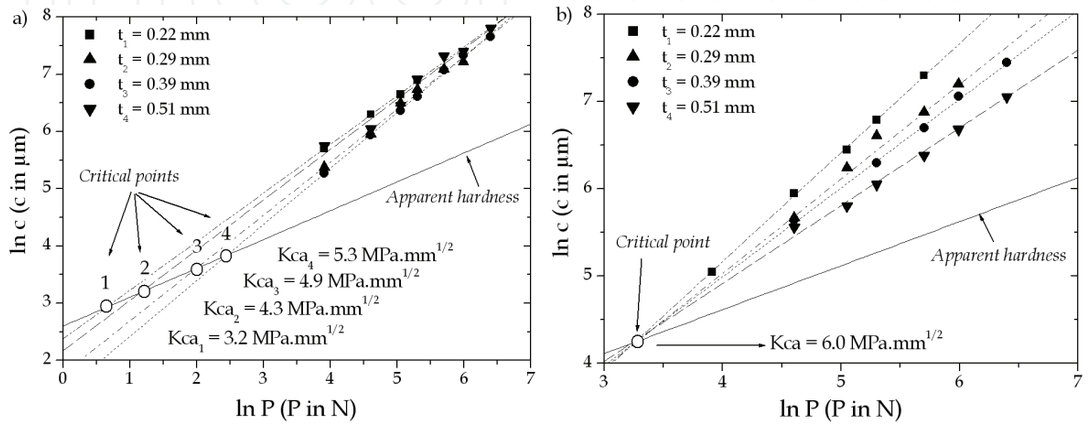


Fig. 23. Interface crack length as a function of the applied load for $Cr_3C_2$/NiCr thick coatings deposited onto a stainless steel for (a) as-received coated materials and (b) for annealed coated materials.

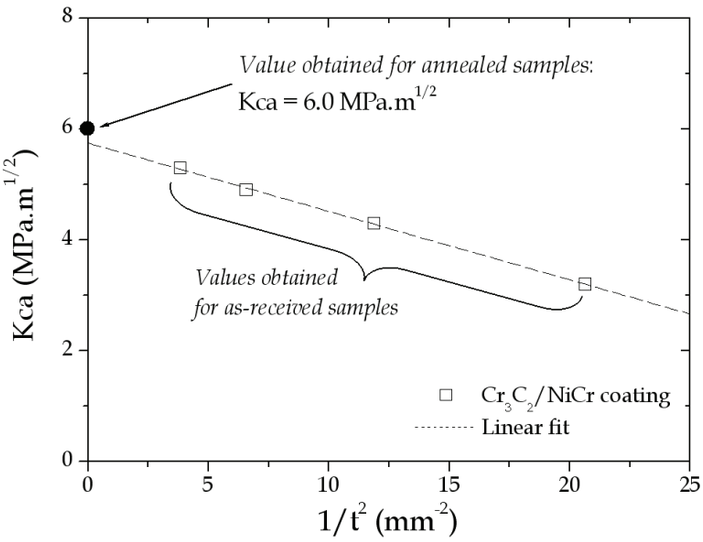


Fig. 24. Interfacial indentation toughness as a function of the coating thickness for as-received and annealed samples.

Figure 23 shows the results of an interfacial indentation test using a Vickers indenter applied to $Cr_3C_2$/NiCr thick coatings deposited on a stainless steel. Figure 23a shows that

the influence of the residual stress on the interfacial indentation toughness depends on coating thickness. It is remarkable that after an annealing treatment which drastically reduces the residual stress state, we obtain a unique value for the interfacial indentation toughness independently of the coating thickness (Figure 23b).
This result is very important as much as the representation of the interfacial indentation toughness for as-received coatings as a function of the coating thickness leads to the value obtained for annealed samples (Fig. 24).
As a main conclusion, this result allows the expression of the interfacial indentation toughness as a function of the residual stress and the absolute toughness which will be obtained for an infinite coating thickness or, consequently, without any residual stress (Lesage and Chicot, 2002):

$$Kca = Kca_0 + \frac{2}{\sqrt{\pi}} \cdot \sigma_R \cdot c_{c_0}^{1/2} \tag{72}$$

where $c_{CO}$ is the critical crack length corresponding to the absolute toughness $Kca_O$ and the residual stresses $\sigma_R$.
From the adhesion characterisation of a thick coating on its substrate, Araujo et al. (2005) reported a detailed discussion of the influence of the residual stress intensity and their repartition throughout the coating on the adhesive properties. In addition, Lesage et al. (2000a, 2000b) discussed the effect of thermal shocks or hydrogen embrittlement on the adhesive properties.

## 7. Conclusion

The indentation test is very useful for determining some mechanical properties but the results must be discussed with particular attention in order to give sound interpretations. As an example:

- For hardness, it is necessary to provide the indentation testing conditions with which the test has been performed. Moreover, a complete determination of the hardness requires two parameters, i.e. the macro-hardness corresponding to the hardness obtained for an infinite load and a characteristic scale-length depending on the models in order to supply the hardness-load variation.
- For the elastic properties, indentation tests lead to the bulk modulus instead of the Young's modulus. The bulk modulus can be determined by Knoop indentation or by analysing the unloading part of a load-depth curve resulting from instrumented indentation tests when applying spherical or conical indenters if some precautions are taken into account like the introduction of the instrument compliance into the reduced modulus calculation.
- For Vickers indentation fracture toughness, numerous relations are able to give a value according to the cracking mode below the indent. Since the experimental determination of the cracking mode is very difficult, we suggest a relationship able to define the cracking mode through an experimental exponent. In addition, two multiplicative coefficients which are material dependent allow the determination of comparable values with those given in the literature.
- For tensile mechanical properties by indentation, two types of approach can be

employed. One of them is based on Hollomon's law or Ludwik's law and the relations between tensile stress-strain and indentation stress-strain; the other groups of relations are those corresponding to the expanding cavity models, taking into account the indenter type and the indentation size effect. In the example shown here, all the models were tested in order to show that without any prior information on the tensile behaviour of the material, it is very difficult to guaranty the true mechanical behaviour. Nevertheless, some models seem to converge toward a unique Ludwik's law representing the tensile plastic domain.

- For adhesive properties, scratch tests and interfacial indentation tests are helpful to give an adhesive parameter. The choice between the two tests is based on the coating thickness and on the coating hardness. In addition for thick coatings, the interfacial indentation test can give additional information like the influence of the residual stresses or thermal treatments effect on the adhesive properties.

## 8. References


Abu Al-Rub, R.K. & Voyiadjis, G.Z. (2004). Analytical and experimental determination of the material intrinsic length scale of strain gradient plasticity theory from micro- and nano-indentation experiments. *International Journal of Plasticity*, Vol. 20, No. 6, 1139-1182.

Alcala, J.; Barone, A.C. & Anglada, M. (2000). The influence of plastic hardening on surface deformation modes around Vickers and spherical indents. *Acta Materialia*, Vol. 48, No. 13, 3451-3464.

Anstis, G.R.; Chantikul, P.; Lawn, B.R. & Marshall, D.B. (1981). A critical evaluation of indentation techniques for measuring fracture toughness : I, Direct Crack Measurements. *Journal of the American Ceramic Society*, Vol. 64, No. 9, 533-538.

Antunes, J.M.; Menezes, L.F. & Fernandes, J.V. (2006). Three-dimensional numerical simulation of Vickers indentation tests. *International Journal of Solids and Structures*, Vol. 43, No. 3-4, 784-806.

Araujo, P.; Chicot, D.; Staia, M.H. & Lesage, J. (2005). Residual stresses and adhesion of thermal spray coatings. *Surface Engineering*. Vol. 21, No. 1, 35-40.

Benayoun, L.; Fouilland-Paillé, J. & Hantzpergue, J. (1999). Microscratch test studies of thin silica films on stainless steel substrates. *Thin Solid Films*, Vol. 352, No. 1-2, 156-166 S.

Benjamin, P. & Weaver, C. (1960). Measurement of adhesion of thin films: Proceedings of the Royal Society, London, Vol. 254 A, pp. 163-176.

Bilodeau, G.G. (1992). Regular pyramid punch problem. *Journal of Applied Mechanics*, Vol. 59, No. 3, 519-523.

Bückle, H. (1973). in: J.H. Westbrook, H. Conrad (Eds.), The Science of Hardness Testing and Its Research Applications, ASME, Metal Park, OH, p. 453.

Bull, S.J.; Page, T.F. & Yoffe, E.H. (1989). An explanation of the identification size effect in ceramics. *Philosophical Magazine Letters*. Vol. 59, No. 6, 281-288.

Bull, S.J. & Rickerby, D.S. (1990). New developments in the modelling of the hardness and scratch adhesion of thin films. *Surface and Coating Technology*, Vol. 42, No. 2, 149-164.

Burnett, P.J. & Rickerby, D.S. (1987a). The mechanical properties of wear-resistant coatings. I. Modelling of hardness behaviour. *Thin Solid Films*, Vol. 148, 41-50.

Burnett, P.J. & Rickerby, D.S. (1987b). The mechanical properties of wear-resistant coatings. II. Experimental studies and interpretation of hardness. *Thin Solid Films*, Vol. 148, 51-68.

Briscoe, B.J.; Sebastian, K.S. & Adams, M.J. (1994). The effect of indenter geometry on the elastic response to indentation. *Journal of Physic D: Applied Physic*, Vol. 27, No. 6, 1156-1162.

Cheng, Y.T. & Cheng, C.M. (2004). Scaling, dimensional analysis, and indentation measurements. *Materials Science and Engineering: R: Reports*, Vol. 44, No. 4-5, 91-149.

Chicot, D. & Lesage, J. (1995). Absolute hardness of films and coatings**.** *Thin Solid films*, Vol. 254, No. 1-2, 123-130.

Chicot, D.; Démarécaux, P. & Lesage, J. (1996). Apparent interface toughness of substrate and coating couples from indentation tests, *Thin Solid Films*, Vol. 283, No. 1-2, 151-157.

Chicot, D.; Mercier, D.; Roudet, F.; Silva, K.; Staia, M.H. & Lesage, J. (2007a). Comparison of instrumented Knoop and Vickers hardness measurements on various soft materials and hard ceramics, *Journal of the European Ceramic Society*, Vol. 27, No. 4, 1905-1911.

Chicot, D.; Roudet, F.; Soom, A. & Lesage J. (2007b). Interpretation of instrumented hardness measurements on stainless steel with different surface preparations. *Surface Engineering*, Vol. 23, No. 1, 32-39.

Chicot, D.; Bemporad, E.; Galtieri, G.; Roudet, F.; Alvisi, M. & Lesage, J. (2008). Analysis of data from various indentation techniques for thin films intrinsic hardness modelling. *Thin Solid Films*, Vol. 516, No. 8, 1964-1971.

Chicot, D. (2009). Hardness length-scale factor to model nano- and micro-indentation size effects, *Materials Science and Engineering: A,* Vol. 499, No. 1-2, 454-461.

Chicot, D.; Roudet, F.; Lepingle, V. & Louis, G. (2009a). Strain gradient plasticity to study hardness behaviour of magnetite (Fe3O4) under multicyclic indentation, *Journal of Materials Research*, Vol. 24, No. 3, 749-759.

Chicot, D.; Duarte, G.; Tricoteaux, A.; Jorgowski, B.; Leriche, A. & Lesage J. (2009b), Vickers Indentation Fracture (VIF) modeling to analyze multi-cracking toughness of titania, alumina and zirconia plasma sprayed coatings, *Materials Science and Engineering: A*, Vol. 527, No. 1-2, 65-76.

Chicot, D.; Gil, L.; Silva, K. ; Roudet, F. ; Puchi-Cabrera, E.S. ; Staia M.H. & Teer, D.G. (2010a). Thin film hardness determination using indentation loading curve modelling. *Thin Solid Films*, Vol. 518, No. 19, 5565-5571.

Chicot, D.; Roudet, F.; Zaoui, A. ; Louis, G. & Lepingle, V. (2010b). Influence of visco-elasto-plastic properties of magnetite on the elastic modulus: Multicyclic indentation and theoretical studies. *Materials Chemistry and Physics*, Vol. 119, No. 1-2, 75-81.

Chong, A.C.M. & Lam, D.C.C. (1999). Strain gradient plasticity effect in indentation hardness of polymers. *Journal of Materials Research*, Vol. 14, No. 10, 4103-4110.

CSM Bulletin (2008). Influence of indenter tip radius on the scratch resistance of an automotive clearcoat. CSM Instruments, Advanced Mechanical Surface Testing, No. 25, February 2008.

Dao, M.; Chollacoop, N.; Van Vliet, K.J.; Venkatesh, T.A. & Suresh, S. (2001). Computational modeling of the forward reverse problems in instrumented sharp indentation. *Acta Materialia*, Vol. 49, No. 19, 3899-3918.

Doerner, M.F. & Nix, W.D. (1986). A method of interpreting the data from the depth-sensing indentation instruments. *Journal of Materials Research*, Vol. 1, No. 4, 601-609.

Durst, K.; B. Backes, B. & Goken, M. (2005). Indentation size effect in metallic materials: Correcting for the size of the plastic zone. *Scripta Materialia*, Vol. 52, No. 11, 1093-1097.

Felder, E. & Laugier, M. (1992). Le test de rayure (scratch test) des produits revêtus, Synthèse bibliographique, mars 1992, Rapport de contrat CEMEF-UNIREC.

Field, J.E. & Telling, R.H. (1999). The Young modulus and Poisson ratio of diamond. Research Note, Cavendish Laboratory, Cambridge.

Fischer-Cripps A.C. (2004). A simple phenomenological approach to nano-indentation creep, *Materials Science and Engineering A*, Vol. 385, No. 1-2, 74-82.

Fischer-Cripps, A.C. (2006). Critical review of analysis and interpretation of nano-indentation test data. *Surface and Coating Technology*, Vol. 200, No. 14-15, 4153-4165.

Gao, X.L. (2006). An expanding cavity model incorporating strain-hardening and indentation size effects. *International Journal of Solids and Structures*, Vol. 43, No. 21, 6615-6629.

Giannakopoulos, A.E.; Larsson, P.L. & Vestergaard, R. (1994). Analysis of Vickers indentation. *International Journal of Solids and Structure*, Vol. 31, No. 19, 2679-2708.

Giannakopoulos, A.E. & Larsson, P.L. (1997). Analysis of pyramid indentation of pressure-sensitive hard metals and ceramics. *Mechanics of Materials*, Vol. 25, No. 1, 1-35.

Gong, J.; Wu, J. & Guan, Z. (1999). Analysis of the indentation size effect on the apparent hardness for ceramics. *Materials Letters*, Vol. 38, No. 3, 197-201.

Gong, J.; Wang, J. & Guan, Z. (2002). A comparison between Knoop and Vickers hardness of silicon nitride ceramics, *Materials Letters.*, Vol. 56, No. 6, 941-944.

Hay, J.C.; Bolshakov, A. & Pharr G.M. (1999). Critical examination of the fundamental relations used in the analysis of nano-indentation data, *Journal of Materials Research*, Vol. 14, No. 6, 2296–2305.

Hays, C. & Kendall, E.G. (1973). Analysis of Knoop hardness. *Metallurgy*, Vol. 6, No. 4, 275-282.

Heavens, O.S. (1950). Some factors influencing the adhesion of films produced by vacuum evaporation. Journal de Physique et le Radium, Vol. 11, No. 7, 355-360.

Herbert, E.G., Pharr, G.M., Oliver, W.C., Lucas, B.N. & Hay, J.L. (2001). On the measurement of stress-strain curves by spherical indentation. *Thin Solid Films*, Vol. 398-399, 331-335.

Hollomon, J.H. (1945). Tensile deformation, *Transactions of the American Institute of Mining and Metallurgical Engineers*, Vol. 162, 268-290.

Huang, Y. Feng, X., Pharr, G.M. & Hwang, K.C. (2007). A nano-indentation model for spherical indenters. *Modelling Simulation Material Science and Engineering*, Vol. 15, No. 1, S255-S262.

Ichimura, H.; Rodriguez, F.M. & Rodrigo, A. (2000). The composite and film hardness of TiN coatings prepared by cathodic arc evaporation. *Surface and Coating Technology*, Vol. 127, No. 2, 138-143.

Jönsson, B. & Hogmark, S. (1984). Hardness measurements of thin films = Mesures de dureté sur des couches minces. *Thin Solid Films*, Vol. 114, No. 3, 257-269.

Karlsson, L., Hultman, L, Sundgren, J.-E., (2000). Influence of residual stresses on the mechanical properties of $TiC_xN_{1-x}$ (x = 0, 0.15, 0.45) thin films deposited by arc evaporation. *Thin Solid Films.* Vol. 371, No. 1-2, 167-177.

Kick, F. (1885). Das Gestez der proportionalen Widerstande und seine Anwendung. Delidzig, Felix.

King, R.B. (1987). Elastic analysis of some punch problems for layered medium. *International Journal of Solids and Structures*, Vol. 23, No. 12, 1657-1664.

Korsunsky, A.M.; McGurk, M.R.; Bull, S.J. & Page, T.F. (1998). On the hardness of coated systems. *Surface and Coating Technology*. Vol. 99, No. 1, 171-183.

Laeng, P. & Steinmann, P.A. (1981). Adhesion testing of hard CVD coatings using the scratch test: Proc. 8th. Int. Conf. CVD 1981, Electrochem. Soc., Pennington, NJ, pp. 723-736.

Larsson, P.L.; Giannakopoulos, A.E.; Söderlund, E.; Rowcliffe, D.J. & Vestergaard, R. (1996). Analysis of Berkovich indentation. *International Journal of Solids and Structure*, Vol. 33, No. 2, 221-248.

Lawn, B.R., Evans, A.G. & Marshall, D.B. (1980). Elastic/plastic indentation damage in ceramics: The median/radial crack system. *Journal of the American Ceramic Society*, Vol. 63, No. 9-10, 574-581.

Lesage, J.; Chicot, D.; Araujo, P.; Zampronio, M. & De Miranda P.E.V. (2000a) Role of hydrogen on adhesion of NiCr thermal sprayed coatings. *Thin Solid Films*, Vol. 377, 675-680.

Lesage, J.; Staia, M.H.; Chicot, D.; Godoy, C. & De Miranda P.E.V. (2000b). Effect of thermal treatments on adhesive properties of a NiCr thermal sprayed coatings. *Thin Solid Films*, Vol. 377, 681-686.

Lesage, J. & Chicot, D. (2002). Role of residual stresses on interface toughness of thermally sprayed coatings. *Thin Solid Films*, Vol. 415, No. 1-2, 143-150.

Lesage, J.; Pertuz, A.; Puchi-Cabrera, E.S. & Chicot, D. (2006). A model to determine the surface hardness of thin films from standard micro-indentation tests. *Thin Solid Films*, Vol. 497, No. 1-2, 232-238.

Li, H. & Bradt, R.C. (1993). The micro-hardness indentation load/size effect in rutile and cassiterite single crystals. *Journal of Materials Research*, Vol. 28, 917-926.

Ludwik, P. (1909). Element der Technologischen Mechanik, Springer Berlin, 32-44.

Marshall, D.B.; Noma, T. & Evans A.G. (1980). A simple method for determining elastic-modulus-to-hardness ratios using Knoop indentation measurements, *Journal of American Ceramic Society*, Vol. 65, No. 10, C175-C176.

Matthews, J.R. (1980). Indentation hardness and hot pressing. *Acta Metallurgica*, Vol. 28, 311-318.

Meyer, E. (1908). Untersuchen über Härteprüfung und Härte. *Z. Ver. deutscher Ing*., Vol. 52, 645-654.

Miranzo, P. & Moya, J.S. (1984). Elastic/plastic indentation in ceramics: a fracture toughness determination method, *Ceramics International*, Vol. 10, No. 4, 147-152.

Mittal, K.L. (1987). Selected bibliography on adhesion measurement of films and coatings. *Journal of Adhesion Science and Technology*, Vol. 1, No. 3, 247-259.

Mukhopadhyay, A. K.; Datta, S. K. & Chakraborty, D. (1990). On the micro-hardness of silicon nitride and sialon ceramics, *Journal of the European Ceramic Society*, Vol. 6, No. 5, 303-311.

Nix, W.D. & Gao, H. (1998). Indentation size effects in crystalline materials: A law for strain gradient plasticity, *Journal of the Mechanics and Physics of Solids*, Vol. 46, No. 3, 411-425.

Oliver, W.C. & Pharr G.M. (1992). An improved technique for determining hardness and elastic modulus using load and displacement sensing indentation experiments, *Journal of Materials Research*, Vol. 7, No. 6, 1564-1583.

Perry, A.J.; Laeng, P. & Steinmann, P.A. (1981). Adhesion measurements on hard thin well-adhering coatings – A Review: Proc. 8th. Int. Conf. CVD 1981, Electrochem. Soc., Pennington, NJ, pp. 475-488.

Ponton, C. B. & Rawlings, D.R. (1989). Vickers indentation fracture toughness test Part 1 Review of literature and formulation of standardized indentation toughness equations. *Materials Science and Technology*, Vol. 5, No. 9, 865-872.

Puchi-Cabrera, E. S. (2002). A new model for the computation of the composite hardness of coated systems. *Surface and Coating Technology*, Vol. 160, No. 2, 177-186.

Qiu, X.; Huang, Y.; Nix, W.D.; Hwang, K.C. & Gao, H. (2001). Effect of intrinsic lattice resistance in strain gradient plasticity. *Acta Materialia*, Vol. 49, No. 19, 3949-3958.

Rajendran, V.; Nishara Begum, A.; Azooz, M. A ; El Batal, F. H. (2002). Microstructural dependence on relevant physical-mechanical properties on $SiO_2$-$Na_2O$-CaO-$P_2O_5$ biological glasses. *Biomaterials*, Vol. 23, No. 21, 4263-4275.

Roman, A. ; Chicot, D. & Lesage, J. (2002). Indentation tests to determine the fracture toughness of nickel phosphorus coatings. *Surface and Coatings Technology*, Vol. 155, No. 2-3, 161-168.

Sangwal, K.; Surowska, B. & P. Blaziak, P. (2002). Analysis of the indentation size effect in the micro-hardness measurement of some cobalt-based alloys. *Material Chemistry and Physic*, Vol. 77, No. 2, 511-520.

Sargent, P.M. (1979). Ph.D. Thesis, University of Cambridge, United Kingdom.

Sekler, J.; Steinmann, P.A. & Hintermann, H.E. (1998). The scratch test: Different critical load determination techniques. *Surface and Coatings Technology*, Vol. 36, No. 1-2, 519-529.

Steinmann, P.A.; Tardy, Y. & Hintermann, H.E. (1987). Adhesion testing by the scratch test method: the influence of intrinsic and extrinsic parameters on the critical load, *Thin Solids Films*, Vol. 154, No. 1-2, 333-349.

Sun, S.; Zheng, S. & Bell, T. (1995). Finite element analysis of the critical ratio of coating thickness to indentation depth for coating property measurements by nano-indentation. *Thin Solid Films*, Vol. 258, No. 1-2, 198-204.

Swift, H.W. (1952), Plastic instability under plane stress. *Journal of Mechanic and Physic of Solids*, Vol. 1, No. 1, 1-18.

Tricoteaux, A.; Duarte, G.; Chicot, D.; Le Bourhis, E.; Bemporad, E. & Lesage J. (2010). Depth-sensing indentation modeling for determination of elastic modulus of thin films, *Mechanics of Materials*, Vol. 42, No. 2, 166-174.

Ullner, C.; Germak, A.; Le Doussal, H.; Morrell, R.; Reich, T. & Vandermeulen, X. (2001). Hardness testing on advanced technical ceramics, *Journal of the European Ceramic Society*, Vol. 21, No. 4, 439-451.

Ullner, C.; Beckmann, J. & Morrell, R. (2002). Instrumented indentation test for advanced technical ceramics, *Journal of the European Ceramic Society*, Vol. 22, No. 8, 1183-1189.

Veprek, R.G.; Parks, D.M.; Argon, A.S. & Veprek, S. (2006). Non-linear finite element constitutive modeling of mechanical properties of hard and superhard materials studied by indentation. *Materials Science Engineering A*. Vol. 422, No. 1-2, 205-217.

Weaver, C. (1975). Adhesion of thin films. *Journal of Vacuum Science and Technology*. Vol. 12, No. 1, 18-25.

Zeng, K. & Chiu, C.-h. (2001). An analysis of load-penetration curves from instrumented indentation. *Acta Materialia*, Vol. 49, No. 17, 3539-3551.

Zhu, T.T., Bushby, A.J. & Dunstan D.J. (2008). Size effect in the initiation of plasticity for ceramics in nano-indentation. *Journal of Mechanics and Physics of Solids*, Vol. 56, No. 4, 1170-1185.

IntechOpen

IntechOpen

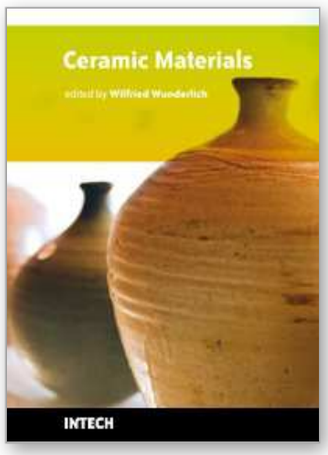


**Ceramic Materials**

Edited by Wilfried Wunderlich

ISBN 978-953-307-145-9

Hard cover, 228 pages

**Publisher** Sciyo

**Published online** 28, September, 2010

**Published in print edition** September, 2010

This is the first book of a series of forthcoming publications on this field by this publisher. The reader can enjoy both a classical printed version on demand for a small charge, as well as the online version free for download. Your citation decides about the acceptance, distribution, and impact of this piece of knowledge. Please enjoy reading and may this book help promote the progress in ceramic development for better life on earth.

**How to reference**

In order to correctly reference this scholarly work, feel free to copy and paste the following:

Didier Chicot and Arnaud Tricoteaux (2010). Mechanical Properties of Ceramic by Indentation: Principle and Applications, Ceramic Materials, Wilfried Wunderlich (Ed.), ISBN: 978-953-307-145-9, InTech, Available from: http://www.intechopen.com/books/ceramic-materials/mechanical-properties-of-ceramic-by-indentation

INTECH
open science | open minds

**InTech Europe**

University Campus STeP Ri
Slavka Krautzeka 83/A
51000 Rijeka, Croatia
Phone: +385 (51) 770 447
Fax: +385 (51) 686 166
www.intechopen.com

**InTech China**

Unit 405, Office Block, Hotel Equatorial Shanghai
No.65, Yan An Road (West), Shanghai, 200040, China
中国上海市延安西路65号上海国际贵都大饭店办公楼405单元
Phone: +86-21-62489820
Fax: +86-21-62489821

© 2010 The Author(s). Licensee IntechOpen. This chapter is distributed under the terms of the Creative Commons Attribution-NonCommercial-ShareAlike-3.0 License, which permits use, distribution and reproduction for non-commercial purposes, provided the original is properly cited and derivative works building on this content are distributed under the same license.

IntechOpen

IntechOpen